

## RESEARCH ARTICLE

10.1002/2017JB014342

## Key Points:

- In situ deformation, slump, and chaotic deposits in the Dead Sea depocenter are seismically triggered
- Source and sedimentary process of the three types of disturbance is determined
- Long sequences of disturbance in a seismically active lake depocenter have the potential to infer earthquake clusters

## Supporting Information:

- Supporting Information S1
- Data Set S1
- Data Set S2

## Correspondence to:

Y. Lu,  
yinlu@post.tau.ac.il;  
yinlusedimentology@yeah.net

## Citation:

Lu, Y., Waldmann, N., Ian Alsop, G., & Marco, S. (2017). Interpreting soft sediment deformation and mass transport deposits as seismites in the Dead Sea depocenter. *Journal of Geophysical Research: Solid Earth*, 122, 8305–8325. <https://doi.org/10.1002/2017JB014342>



Received 18 APR 2017

Accepted 9 OCT 2017

Accepted article online 13 OCT 2017

Published online 30 OCT 2017

## Interpreting Soft Sediment Deformation and Mass Transport Deposits as Seismites in the Dead Sea Depocenter

Yin Lu<sup>1,2,3</sup> , Nicolas Waldmann<sup>2</sup>, G. Ian Alsop<sup>4</sup>, and Shmuel Marco<sup>1</sup> 

<sup>1</sup>Department of Geophysics, Tel Aviv University, Tel Aviv, Israel, <sup>2</sup>Dr. Moses Strauss Department of Marine Geosciences, Leon H. Charney School of Marine Sciences, University of Haifa, Haifa, Israel, <sup>3</sup>Now at Sedimentology and Marine Paleoenvironmental Dynamics Group, Institute of Earth Sciences, Heidelberg University, Heidelberg, Germany, <sup>4</sup>Department of Geology and Petroleum Geology, University of Aberdeen, Aberdeen, UK

**Abstract** We have studied the history of earthquakes over the past 70 kyr by analyzing disturbed sedimentary layers around the margins of the Dead Sea. However, we know little about disturbances in the basin depocenter, where water depth is ~300 m, and accessible only by drilling. In this study, we compare disturbances from the Dead Sea depocenter, with the contemporaneous earthquake record (~56–30 ka) that was recovered on the western margin of the lake. This comparison allows us to discern the characteristics of disturbance in the different subaqueous environments and identify the source and sedimentary process of mass transport deposits. Our observations indicate that (i) the long disturbance sequences in the Dead Sea depocenter are composed of in situ deformation, slump, and chaotic deposits; (ii) earthquake-triggered Kelvin-Helmholtz Instability is a plausible mechanism for the in situ deformation in the lake center; (iii) the slump is slope area sourced; (iv) the unit of chaotic deposits is lakeshore sourced; and (v) earthquake-triggered slope instability is a viable mechanism for the slump and chaotic deposits. We further suggest that long sequences of disturbance in seismically active lake depocenters can be used to infer earthquake clusters.

**Plain Language Summary** In order to extend the Dead Sea Fault earthquake record to preinstrumental time, we need to understand the processes that create disturbance in the basin depocenter where water depth is hundreds of meters. Here we report two disturbed sequences (4–22 m thick) that were drilled in the Dead Sea depocenter. We propose a seismic trigger based on the temporal correlation with previously established earthquake records in the Dead Sea margin. Three basic types of disturbance are defined: in situ deformation, slump, and chaotic deposits (mud-supported gravel). Our observations indicate that (i) earthquake-triggered Kelvin-Helmholtz Instability is a plausible mechanism for the in situ deformation in the Dead Sea depocenter; (ii) slumps are sourced in the slope area; (iii) chaotic deposits (mud-supported gravel) originate nearshore; and (iv) earthquake-triggered slope instability creates slump and chaotic deposits. Our results have widespread implications for studies of sediment disturbance in seismically active lakes, and we further suggest that long sequences of disturbance in such seismically active depocenters can be used to infer patterns of earthquake temporal distributions.

## 1. Introduction

Disruption of unlithified sediments in lacustrine environments provides a valuable archive of past earthquakes. Very few lakes have receded continuously for many millennia, exposing long sedimentary records, like the Dead Sea. The highest pre-Dead Sea sediments are at –165 m (Torstein et al., 2013), whereas the 2017 lake level is at –433 m. Seismic disturbance during the past ~70 kyr in the exposed margins of the lake have been intensively investigated and are therefore relatively well understood (Alsop & Marco, 2011; Alsop, Marco, et al., 2017). However, to date, we know very little about the processes associated with mass transport deposits and their seismological implications in the basin depocenter where water depth is hundreds of meters (~300 m). In this study, we compare the record of disturbed sediments observed in the Dead Sea deep drill core, located at the lake depocenter, with disturbed lake sediments described in the Lisan Formation (Fm) from the lake margins (Alsop & Marco, 2011; Marco & Agnon, 1995). This comparison allows us to delineate the deformation characteristics in the different subaqueous environments, identify the sources of mass transport deposits, and provide a reference for interpreting lacustrine records in seismically active regions.

Soft-sediment deformation is a disruption of unlithified sediments (Alsop et al., 2017; Owen et al., 2011; Van Loon, 2009) and is widely documented in both subaerial (McKee et al., 1971; Moretti, 2000; Pedersen et al., 2015) and subaqueous environments (Avşar et al., 2016; Gladkov et al., 2016; Jiang et al., 2016; Sims, 1973). Commonly, the disturbances are triggered either by seismic shaking (Liu-Zeng et al., 2015; Monecke et al., 2007; Sakaguchi et al., 2011; Sims, 2013; Strasser, Kölling, et al., 2013) or by nonseismic triggers, for example, tides (Greb & Archer, 2007), storm waves (Molina et al., 1998), floods (Li et al., 1996), and sediment overloads (Moretti et al., 2001; Moretti & Sabato, 2007). These disturbances have been used to interpret paleoseismic and paleoclimatic events. In addition, studies of sediments that were disturbed by seismic shaking (seismites) provided off-fault paleoseismic preinstrumental records that span many seismic cycles (Kagan et al., 2005; Ken-Tor et al., 2001; Marco et al., 1996; Migowski et al., 2004).

The location of the Dead Sea Basin within the Dead Sea transform fault zone makes the soft lacustrine sediments deposited in the basin excellent recorders of disturbances. Seilacher (1984) and El-Isa and Mustafa (1986) hypothesized that convolute strata in the Lisan Fm represent earthquake-triggered deformation. Marco and Agnon (1995, 2005) discovered breccia layers juxtaposed against syndepositional faults in the Lisan Fm, thereby proving the seismic origin of those disturbances. Further, Enzel et al. (2000), Ken-Tor et al. (2001), Migowski et al. (2004), and Kagan et al. (2011) provided additional support by correlating documented historical earthquakes with individual seismites.

These previous works are limited to outcrops in the Dead Sea margins, where the lake was relatively shallow and which are now exposed. In this paper, we present two sequences of disturbances in the Lisan Fm recovered from the Dead Sea depocenter during the 2010–2011 International Continental Scientific Drilling Program (ICDP), Dead Sea Deep Drilling Project (DSDDP) (Stein et al., 2011). Our study aims to (1) characterize the imprint of seismic shaking on sediments within the lake depocenter and (2) determine the potential source regions and sedimentary processes responsible for different types of disturbance.

## 2. Geological Setting

### 2.1. Dead Sea Transform

The Dead Sea Transform (also called Dead Sea Fault) is a ~1,000 km long sinistral boundary between the African and Arabian plates, which transfers the Red Sea spreading in the south to the convergence zone along the Taurus-Zagros belt in the north (Garfunkel, 2014) (Figure 1a). It is associated with several pull-apart basins (Garfunkel, 1981, 2014; Garfunkel & Ben-Avraham, 1996), in which the Dead Sea is the deepest continental structure. Left lateral offset of approximately 105 km since the early to middle Miocene is indicated by numerous displaced geological markers (Bartov et al., 1980; Freund et al., 1968; Garfunkel, 1981, 2014).

### 2.2. Seismic Activity Along the Dead Sea Transform

Approximately one century of seismic monitoring along the Dead Sea Transform reveals that most earthquakes are relatively weak (Garfunkel, 2009). The two strongest seismic shocks recorded in modern times occurred at the Gulf of Aqaba (southernmost Dead Sea Transform) on 22 November 1995, with  $M_w = 7.3$  (Klinger et al., 1999), and in the Jericho Valley on 11 July 1927, with  $M_L = 6.2$  (Shapira et al., 1993). Tens of earthquakes with  $M_L > 6$  occurred along the Dead Sea Transform during the past ~3 kyr and are recorded in written documents (Ambraseys, 2009; Amiran et al., 1994; Ben-Menahem, 1991).

Late Holocene records of seismicity are based on documented historical earthquakes and geological archives of intraclast breccia layers that are exposed in the Dead Sea margin area (Kagan et al., 2011; Ken-Tor et al., 2001; Migowski et al., 2004). Observations of intraclast breccia layers that are associated with syndepositional faults extend the earthquake record to ~70 ka based on 36 seismites in the Lisan Fm documented from outcrops in the Perazim Valley (PZ1, Figure 1b) (Agnon et al., 2006; Begin et al., 2005; Marco & Agnon, 1995; Marco et al., 1996). More records are also obtained from 38 earthquake-induced rockfalls in the Soreq and Hartuv Caves (Figure 1b), which span ~184–5 ka (Kagan et al., 2005).

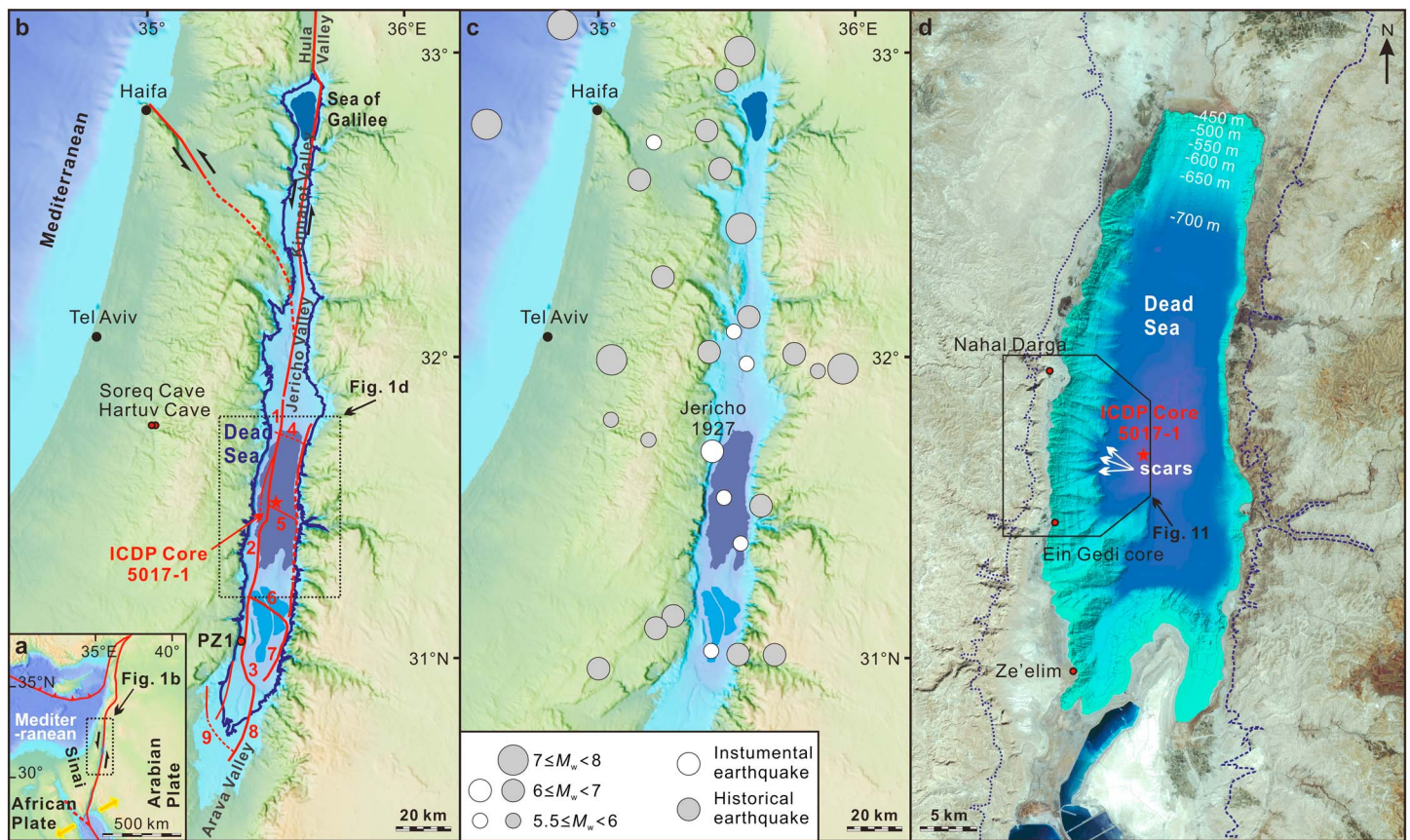


**Figure 1.** Geological setting of the Dead Sea graben and location of ICDP core 5017-1. (a) Plate tectonic setting (Garfunkel, 1981; ten Brink & Ben-Avraham, 1989). (b) Active faults along Dead Sea Fault (Garfunkel, 1981; ten Brink & Ben-Avraham, 1989; Garfunkel & Ben-Avraham, 1996) and position of drill core 5017-1 located in the depocenter of the basin. The light blue area around the Dead Sea Basin indicates the region that is below sea level; the dashed blue line within the light blue area shows the maximum extent of Lake Lisan (lake level was at  $-165$  m) during the Last Glacial Maximum (Torfstein et al., 2013); red points (circled by black lines) mark locations referred to in this study; PZ1: Perazim Valley, section 1; numbers in the figure: 1, Jericho fault; 2, Sedom Fault; 3, Amazyahu Fault; 4, Kalia Fault; 5, En Gedi Fault; 6, Boqeq Fault; 7, Ghor Safi Fault; 8, Arava Fault; and 9, Idan Fault. (c) Instrumental and historical seismicity in the Dead Sea graben and surrounding areas (modified after Migowski et al., 2004). (d) Dead Sea bathymetric map (from Sade et al., 2014). The black box marks the area used in Figure 11; red points (circled by black lines) mark places referred to in this study; the blue dashed lines mark the maximum extent of Lake Lisan during the Last Glacial Maximum.

### 2.3. Sedimentary Regime in the Dead Sea Basin

The Dead Sea basin is the largest and deepest continental pull-apart basin along the Dead Sea Transform (Figure 1b), with a length of approximately  $\sim 150$  km, and width of 15–20 km (Garfunkel, 1981). Sediment began filling the basin in the early Miocene (Al-Zoubi & ten Brink, 2002; Ten Brink & Ben-Avraham, 1989), with a maximum thickness of  $\sim 10$  km (Manspeizer, 1985). In the area of the Dead Sea, this stratigraphy has been divided into six major units: the Hazeva Group ( $N_1$ ) (oldest), Sedom Fm ( $N_2$ ), Amora Fm ( $Q_1$ -MIS 6), Samra Fm (MIS 5), Lisan Fm (MIS 4-2), and Ze'elim Fm (MIS 1) (youngest). The Hazeva Group comprises a  $\sim 2$  km succession of continental red beds deposited in basins south of the Dead Sea and in the Negev desert (Calvo & Bartov, 2001; Sneh, 1981). Following this unit, the Sedom Fm is a thick sequence of mainly marine evaporites with some clastic sediments deposited in an inland lagoon (Manspeizer, 1985).

Subsequently, the Dead Sea Basin has been occupied by a sequence of terminal water bodies during the Quaternary: Lake Amora ( $Q_1$ -MIS 6), Lake Samra (MIS 5), Lake Lisan (MIS 4-2), and the current Dead Sea (MIS 1) (Neev & Emery, 1967; Stein, 2001). During the Last Glacial Maximum, Lake Lisan extended over 240 km N-S, with a lake level at  $-165$  m (Bartov et al., 2002; Torfstein et al., 2013) and is known as the largest lacustrine system (Begin et al., 1974). Primary facies of the Lisan Fm are characterized by alternating laminae of aragonite and detritus (Neugebauer et al., 2014; Schramm et al., 2000). Previous studies conclude that dark



detritus laminae, which consist mainly of fine-grained quartz and calcite grains, were deposited during rainy seasons, while the white aragonite laminae are precipitated during dry seasons (Katz et al., 1977; Prasad et al., 2004; Stein et al., 1997).

### 3. Materials, Methods, and Chronology

#### 3.1. Materials

Between November 2010 and March 2011, a 456.7 m long composite core (core 5017-1) was extracted under the umbrella of the ICDP from a water depth of 297.5 m in the abyssal plain of the Dead Sea depocenter, (31°30'29"N, 35°28'16"E; Figures 1b and 1d). The hydraulic piston coring system was used to drill the upper 30 m, an extended-nose was adopted to recover the remaining deeper part of the core (Stein et al., 2011). The core penetrated the upper part of the Amora Fm (~456.7–328.0 m), Samra Fm (~328.0–177.0 m), Lisan Fm (~177.0–89.3 m), and Ze'elim Fm (~89.3–0 m) (Torfstein et al., 2015), with an average recovery of ~84.5%. In this study, we focus on the Lisan Fm where white and dark lamination can serve as a sensitive stratigraphic marker for seismic events. We evaluate the imprint of seismic shaking on the lacustrine sediments and analyze their sedimentary processes. Further comparison with an outcrop in the Perazim Valley (PZ1, Figure 1b) was carried out as this site archives a long and chronologically well constrained earthquake record (Begin et al., 2005; Marco & Agnon, 1995; Marco et al., 1996). The top of the ~38.5 m thick PZ1 section is at ~267.6 m (Schramm et al., 2000). The section is composed of aragonite-detrital laminae and a few centimeter thick sand and clay layers (Marco et al., 1996; Schramm et al., 2000). A hiatus in sedimentation occurred between ~49.0 ka and 43.8 ka, during a low lake level period (Haase-Schramm et al., 2004).

#### 3.2. Methods

The approaches in the current study include magnetic susceptibility analyses, measured with a Multi-Sensor Core Logger (from Geotek) utilizing a Bartington MS2E sensor at a 1 mm scale resolution on a split core surface. Further elemental analyses of major elements were measured in counts per second (cps) at 1 mm step on the archived halves utilizing an ITRAX  $\mu$ XRF spectrometer. A chromium tube was applied with 30 kV voltage and 30 mA current, with a step size defined at 200  $\mu$ m and an exposure time of 10 s per step. Both petrophysical and geochemical measurements were carried out at the GFZ laboratory facilities in Potsdam. From the different elements measured with the  $\mu$ XRF spectrometer, Ca and Fe were used for the purpose of this study, as Ca best shows the distribution of aragonite and Fe has close relationships to the magnetic susceptibility measurements.

#### 3.3. Chronology

Previous studies by Torfstein et al. (2015) and Kitagawa et al. (2017) anchor the chronology of core 5017-1 by means of U-Th and  $^{14}\text{C}$  methods, respectively. While the  $^{14}\text{C}$  dating was performed on terrestrial plant remains to avoid a potential hard-water effect (Kitagawa et al., 2017), the U-Th dating was carried out on primary aragonites (aragonite laminae) (Torfstein et al., 2015). The age of core 5017-1 ranges from ~220.0 ka to the present (Kitagawa et al., 2017; Neugebauer et al., 2014; Torfstein et al., 2015). The Lisan Fm interval of ~180.0–90.0 m is dated at ~70.0–14.1 ka (Figure 2a) based on six  $^{14}\text{C}$  ages with  $1\sigma$  error (Kitagawa et al., 2017; Neugebauer et al., 2014) and three U-Th ages with  $2\sigma$  error (Torfstein et al., 2015). An age-height plot of the PZ1 outcrop (~70–14 ka) that is based on the work of Haase-Schramm et al. (2004) is provided for comparison (Figure 2) with the chronology of core 5017-1.

In order to calculate ages for intraclast breccias in the PZ1 outcrop, a previously published U-Th data set was utilized. According to Haase-Schramm et al. (2004), the regression age  $A$  (ka) of each intraclast breccia layer in the PZ1 outcrop is calculated as

$$1. \quad 0.8 < H < 17.7,$$

$$A = -0.6338 \times H + 60.18 \quad (1)$$

$$2. \quad 17.7 < H < 38.49,$$

$$A = -1.400 \times H + 68.54 \quad (2)$$

where  $H$  (m) is the height of middle point of each intraclast breccia layer. Error for the regression ages are ~0.8 kyr (Haase-Schramm et al., 2004).



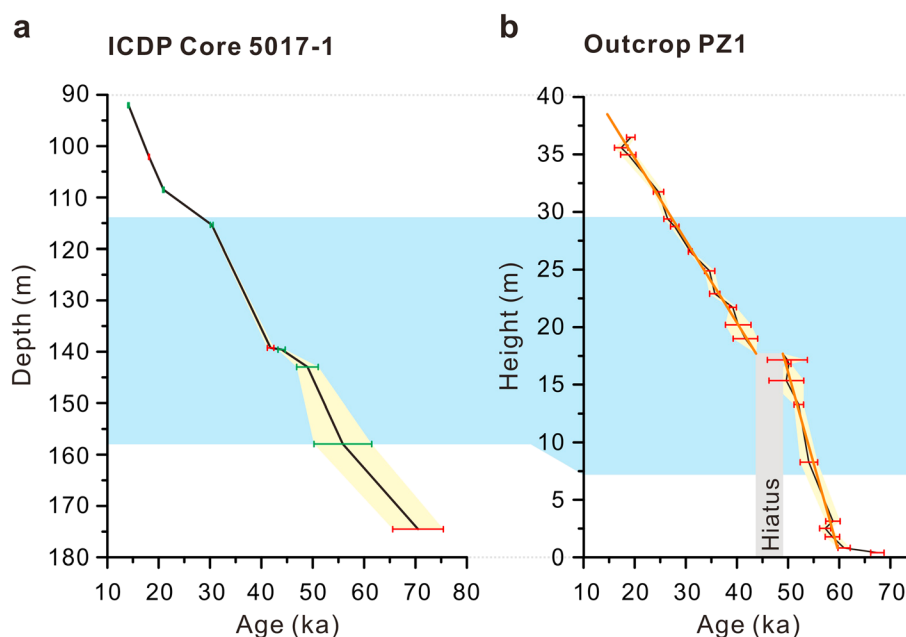


**Figure 2.** Age model of the studied interval in ICDP core 5017-1 and PZ1 outcrop (Figure 1b). The focused section intervals are highlighted by the light blue color. (a) Age-depth plot for the interval of ~180–90 m (Lisan Fm) in core 5017-1 based on six  $^{14}\text{C}$  ages (green bars) (Kitagawa et al., 2017; Neugebauer et al., 2014) and three U-Th ages (red bars) (Torfstein et al., 2015). (b) Age-height plot for the ~38.5 m thick PZ1 outcrop based on U-Th age dating (red bars). Black lines show the isochron age model based on 22 isochron ages; the bold orange lines show the regression age model based on 26 regression ages (regression of height versus age) (Haase-Schramm et al., 2004).

## 4. Results and Observations

### 4.1. Lithofacies

Two disturbed sequences were identified in the core: Sequence I and II (at depths of ~153.9 m to 149.4 m and ~137.5 m to 115.9 m, respectively; Figure 3). Sequence I is characterized by disruption of detritus layers, while Sequence II is marked by disruption of aragonite-detritus laminae. The  $\mu\text{XRF}$  element scanning of Ca and Fe, and magnetic susceptibility generally show high amplitudes of variation across the two sequences (Figures 3b–3d).

We divide the undisturbed sediments into two types of lithofacies: (i) homogeneous mud (Figures 4a and 4b) and (ii) alternating laminae of aragonite and detritus interbedded with homogeneous mud (Figures 4c and 4d). The lithofacies comprising homogeneous mud displays nearly constant values of Ca, Fe, Ca/Fe ratio, and magnetic susceptibility. The lithofacies with alternating laminae of aragonite and detritus shows some minor variations in both Ca, Fe, Ca/Fe ratio, and magnetic susceptibility. The Ca, Fe, and Ca/Fe ratio clearly corresponds with the occurrence of evaporate sequences (aragonite laminae and gypsum layers) in the undeformed core intervals.

### 4.2. Three Basic Types of Disturbance

We classify the two sequences into three basic types of disturbance. Each type shows distinct structures and textures, indicating different geological processes.

1. Type 1. This comprises slightly deformed (Figure 5a) and folded (Figures 5b–5h) aragonite-detritus laminae. Aragonite laminae are well preserved and can be traced around folds and also across microfaults that are developed in some intervals (Figures 5c–5h). In several instances, ~10–25 cm thick turbidites are deposited above deformed units (Figures 5f–5h). These turbidite layers are not disturbed and are not part of the folded aragonite-detritus laminae. However, aragonite-detritus laminae immediately below these turbidites remain undeformed.
2. Type 2. This type comprises intensely deformed aragonite-detritus laminae (Figure 6). Most of the aragonite laminae are fragmented, with the deformed sediments showing distinctive features of plastic flow including folding and attenuation of layering.

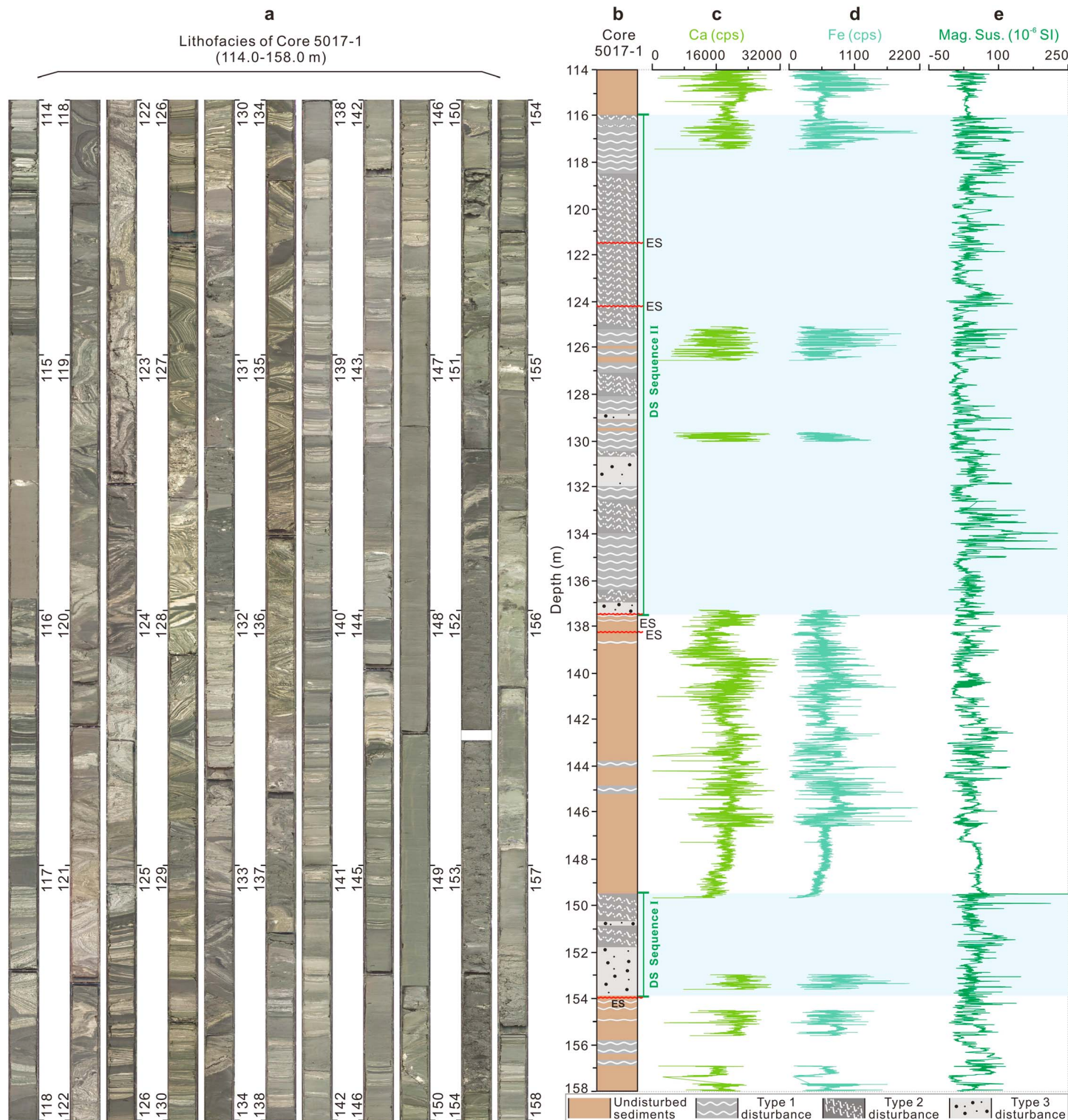


**Figure 3.** Lithofacies and features of focused core interval (114–158 m) in the Dead Sea depocenter. (a) Core images showing the disturbed and undisturbed facies (high-resolution images are shown in Figures 4–7; microcharacteristics of different structures are shown in supporting information Figures S1 and S2). (b) Two meter scale disturbed (DS) sequences are identified by sedimentary structures; ES, erosion surface. Please refer to sections 4.2 and 5.1 for the description and interpretation of the three basic types of disturbance. (c and d)  $\mu$ XRF profiles of Ca, Fe in counts per second (cps). (e) Magnetic susceptibility (Mag. Sus.) data. The light-green shaded areas indicate the corresponding intervals of DS Sequence I and II in Figure 3b.



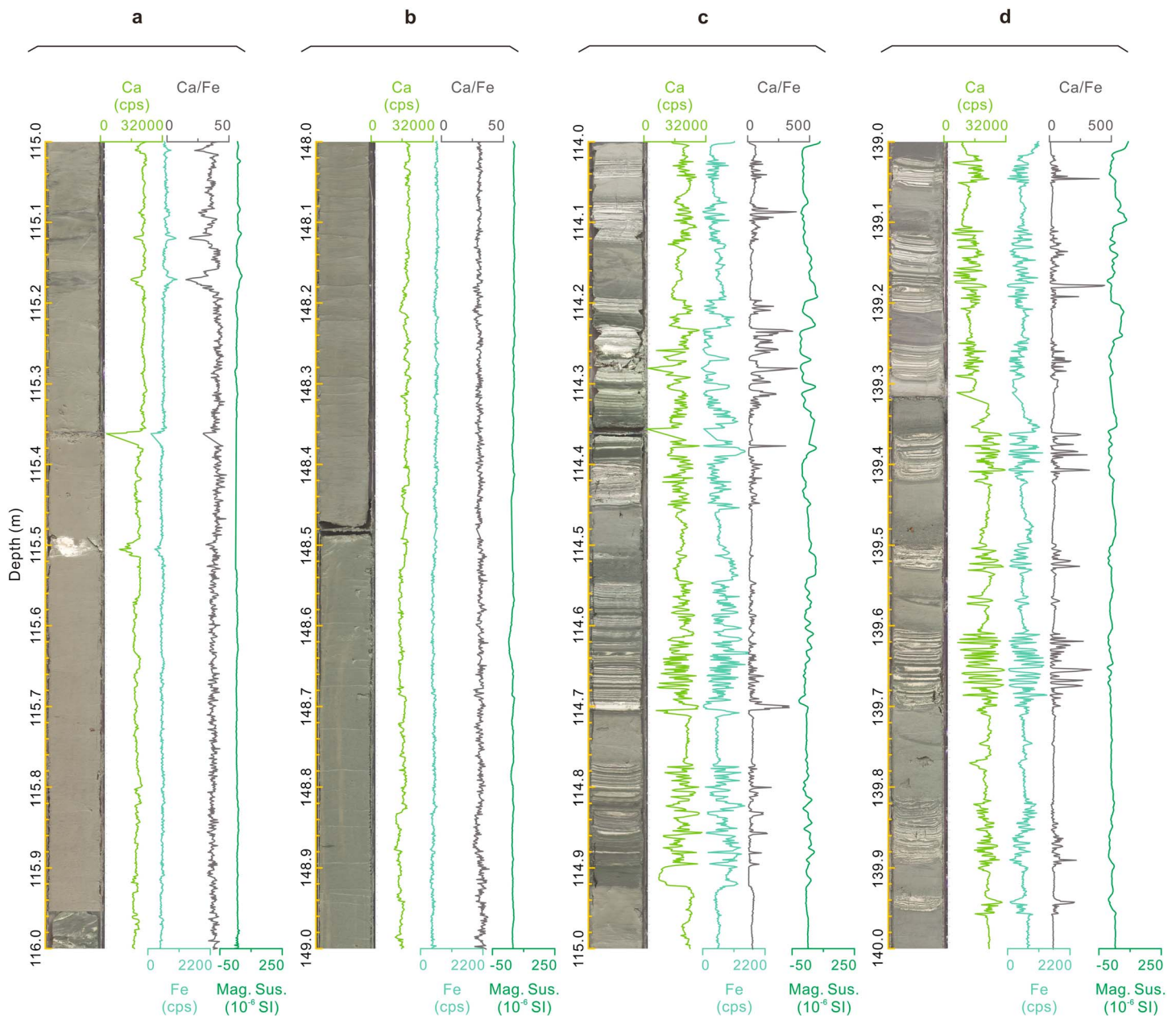


**Figure 4.** Representative lithofacies and features of undisturbed sediments above or below the meter-scale disturbances. (a and b)  $\mu$ XRF profiles of Ca and Fe, magnetic susceptibility data, and sedimentary structures showing the undisturbed sediments of homogeneous mud. (c and d)  $\mu$ XRF profiles of Ca and Fe, magnetic susceptibility data, and sedimentary structures showing undisturbed sediments of alternating lamina of aragonite and detritus.

3. Type 3. Mud that contains coarse sands and ~2–3 cm thick, mostly well-rounded gravels and few laminated intraclasts (Figure 7), showing poorly sorted chaotic structures.

Multiple successions of Types 1, 2, and 3 disturbance were observed within disturbed Sequences I and II. (i) Type 1 at the base, Type 3 in the middle, and Type 2 on the top (e.g., ~132.5–130.4 m); (ii) erosion surface instead of Type 1 at the base, Type 3 in the middle, and Type 2 on the top (~153.9–150.9, ~137.5–136.4 m); (iii) Type 3 at the base, Type 2 on the top (e.g., ~150.9–149.4 m); and (iv) Type 1 at the base, Type 2 on the top (e.g., ~136.4–134.0 m and ~126.0–118.5 m).

#### 4.3. Drilling Artifacts—Angular Discordances

Drilling artifacts that resulted in “angular discordances” across discrete artificial breaks (Figure 8) were identified from disturbed Sequence II. Artificial breaks are visible in thicker deformed units (Type 1 and



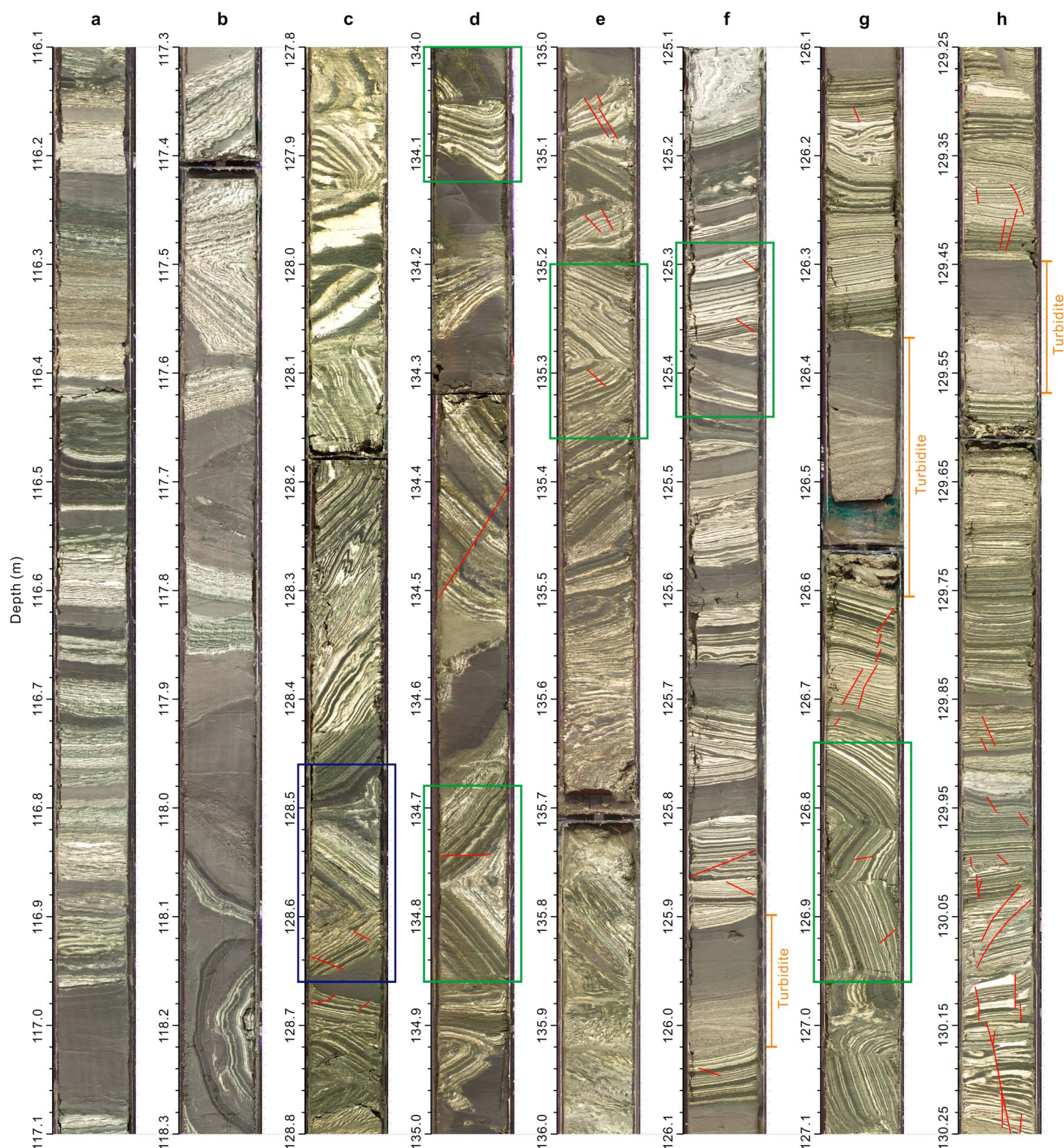


**Figure 5.** Images from core 5017-1 showing Type 1 disturbance in the Dead Sea depocenter. Laminations of aragonite and detritus can be traced in Type 1 disturbance. (a) Deformed laminae of aragonite (core depth: 116.1–117.1 m). (b–h) Folds (core depth: 117.3–118.3 m, 125.1–127.1 m, 127.8–128.8 m, 129.25–130.25 m, and 134.0–136.0 m). (c–h) Microfaults (red lines); (f–h) turbidites are shown as orange line segments. These turbidites do not display evidence of erosion at their base. Moreover, these turbidite layers are not parts of folded aragonite-detritus laminae, that is, not a repetition of former turbidite layers. The blue box indicates angular discordance shown in Figure 8d, and the green boxes mark angular discordances shown in supporting information Slide S1.



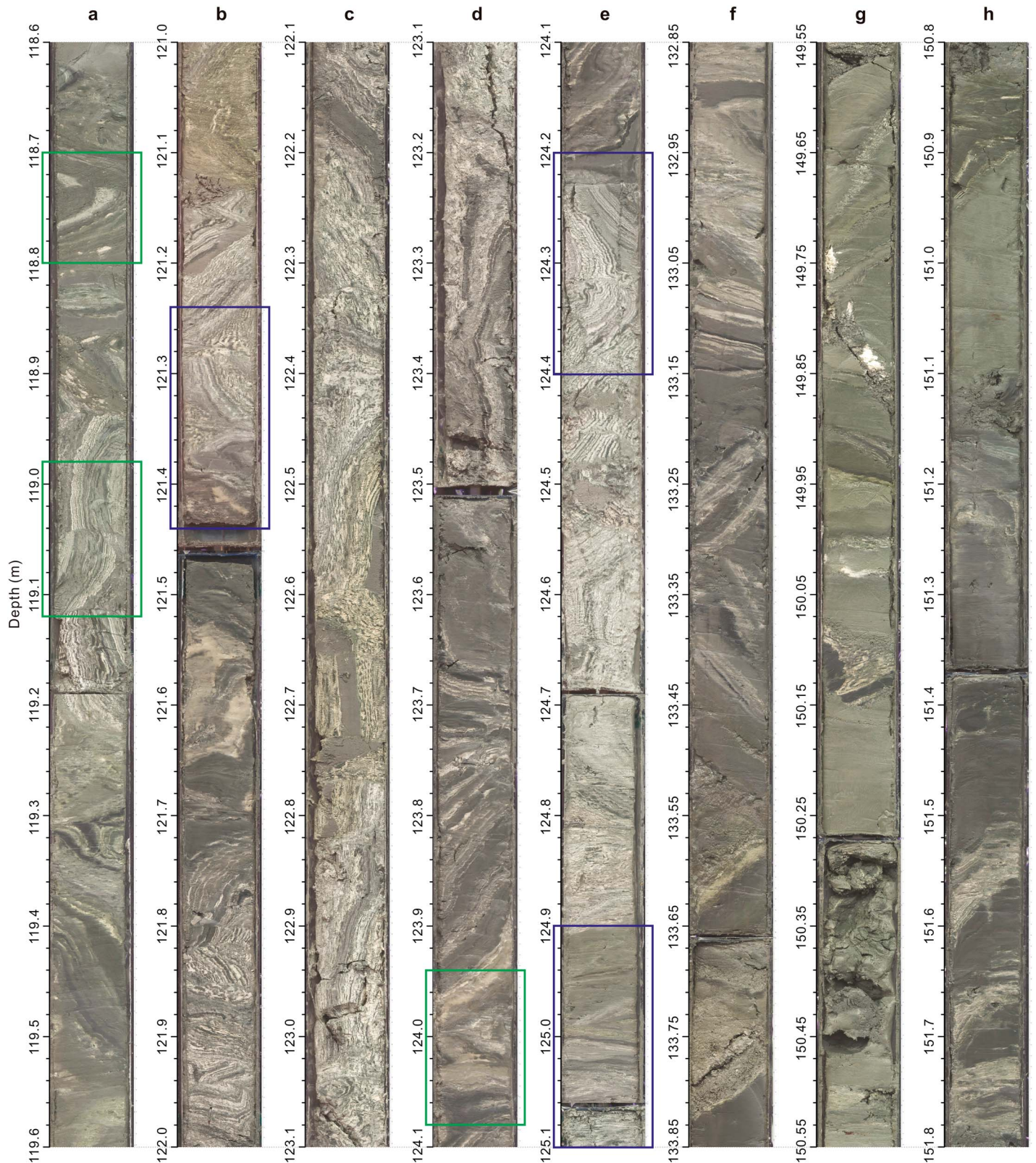


**Figure 6.** Images from core 5017-1 showing Type 2 disturbance in the Dead Sea depocenter. (a–e) Laminations of aragonite are intensely deformed (core depth: 118.6–119.6 m, 121.0–122.0 m, and 122.1–125.1 m). (f–h) The disturbances are mainly composed of mud and sands, with some scattered aragonite laminae (core depth: 132.85–133.85 m, 149.55–150.55 m, and 150.8–151.8 m). The blue boxes indicate the angular discordance shown in Figures 8a–8c, and the green boxes indicate the angular discordances shown in supporting information Slide S1.



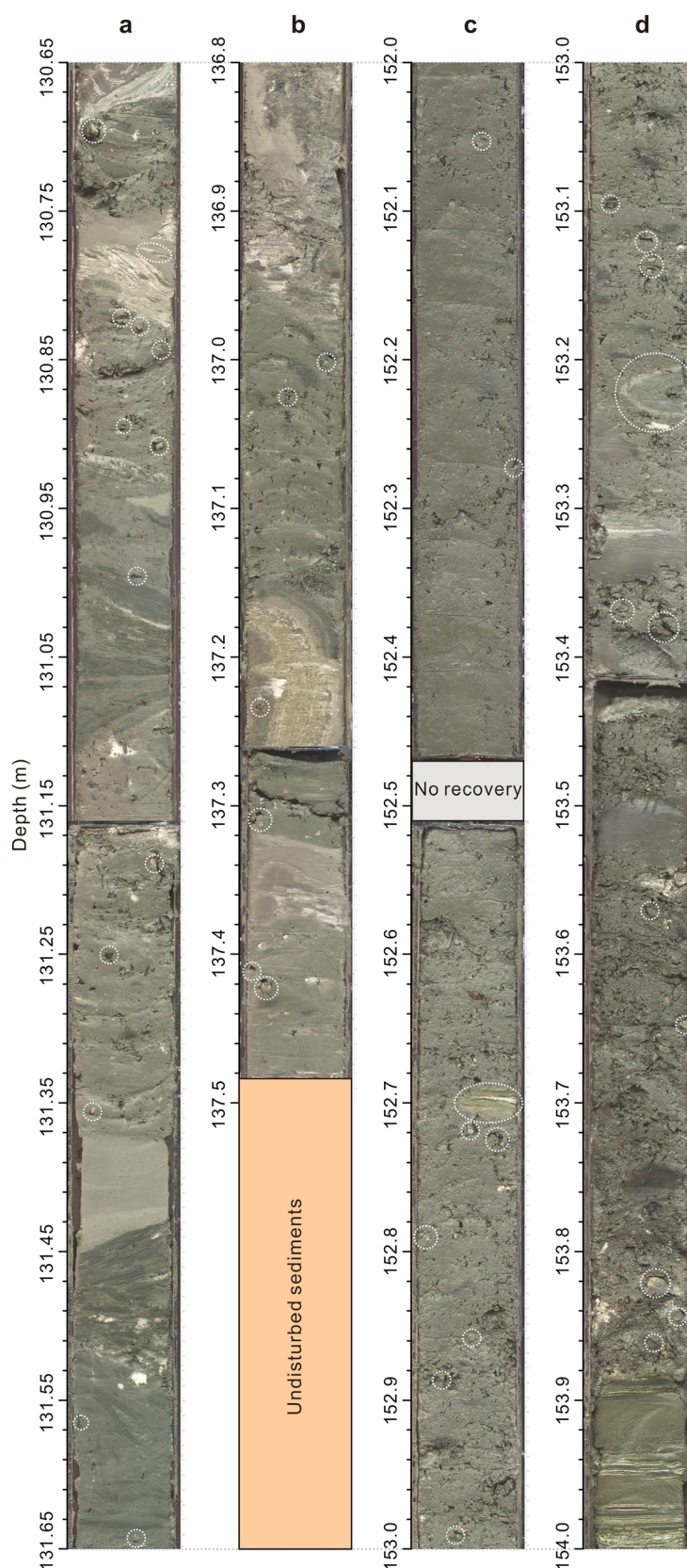


**Figure 7.** Images from core 5017-1 (core depth: 130.65–131.65 m, 136.8–137.5 m, and 152.0–154.0 m) showing Type 3 disturbance (poorly bedded, unsorted strata) in the Dead Sea depocenter. (a–d) Gravels, coarse sands, and intraclasts (Figures 7a, 7c, and 7d) are indicated by the white circles.



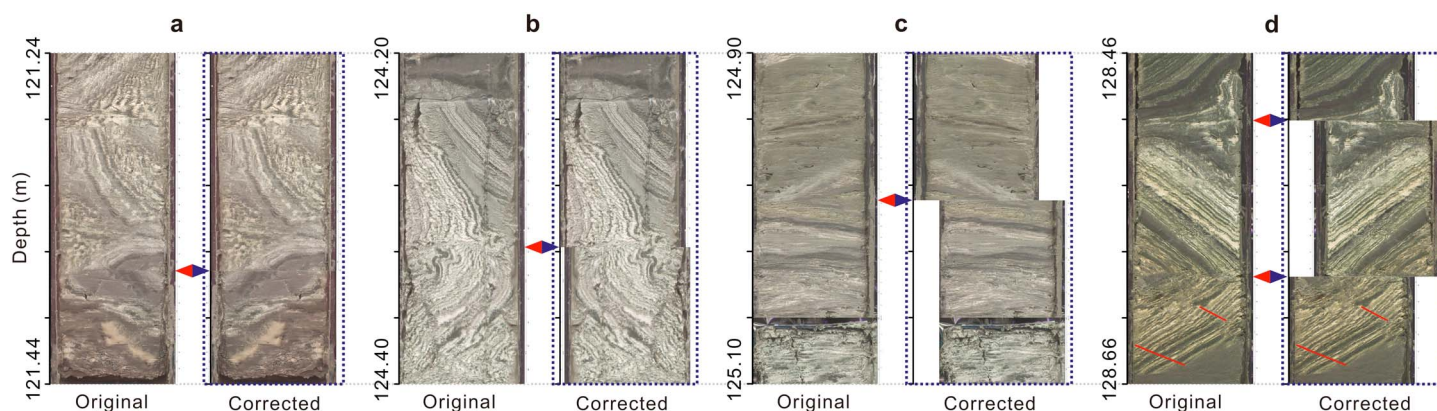


**Figure 8.** Images from core 5017-1 showing typical artificial breaks with rotations of  $\sim 180^\circ$  that were induced by the drilling process. (a–c) Angular discordances (see Figure 6 for their locations) within Type 2 disturbance. (d) Angular discordances (see Figure 5 for its location) within Type 1 disturbance. Please note in each small figure (Figures 8a–8d), the left side is the original image, while the right side is the corrected and restored image. See supporting information Slide S1 for more examples of angular discordances across artificial breaks with rotations of  $\sim 90^\circ$  and  $\sim 180^\circ$ .

Type 2 disturbance) within the disturbed Sequence II (Figures 5 and 6). Angular discordances occur at very regular intervals ( $\sim 5$ – $10$  cm spacing) within each deformed unit (approximately tens of centimeters to meters thick) (Figures 5 and 6). These unnatural angular breaks may be “restored” by rotating the core on each side so that well-defined laminae coincide, resulting in more natural looking folds and slumps after correction. These artificial breaks may accommodate rotations of  $>0$  to  $180^\circ$  relative to their original positions. Artificial breaks with rotations of  $\sim 90^\circ$ , and more examples with rotations of  $\sim 180^\circ$  are shown in the supporting information, Slide S1. In the case of a  $\sim 180^\circ$  rotation, the deformation can be restored by simply mirroring one of the rotated sediment packages (Figure 8 and supporting information Slide S1). In the case of a  $\sim 90^\circ$  rotation, deformation can often be restored by rotating one of the packages (supporting information Slide S1). In the case of any other angle, restoring the deformation is not possible based on 2-D images.

#### 4.4. Temporal Correlation of Disturbed Sequences to Large Earthquake Clusters

Previous paleoseismic studies carried out on Dead Sea outcrops (Agnon et al., 2006; Enzel et al., 2000; Ken-Tor et al., 2001; Marco et al., 1996; Migowski et al., 2004) and speleothems of the Soreq and Har-Tuv Caves in nearby regions (Kagan et al., 2005) proposed that strong earthquakes are clustered over a variety of time scales. Earthquake clusters appear to occur in many other settings, such as in the El Asnam strike fault system in the Algerian margin (Babonneau et al., 2017) and the North Anatolia transform boundary in the Marmara Sea (McHugh et al., 2014). To define earthquake clustering, Kagan and Jackson (1991) proposed a coefficient of variation (COV):

$$\text{COV} = \frac{\sigma_T}{\bar{T}} \quad (3)$$

where  $T$  is the earthquake recurrence time,  $\sigma_T$  is the standard deviation of  $T$ , and  $\bar{T}$  is the average recurrence time. Earthquake distribution with a  $\text{COV} > 1$  indicates clustered earthquakes, whereas distributions with a  $\text{COV} = 1$  indicates random earthquake recurrence, distributions with a  $\text{COV} < 1$  indicates quasiperiodic earthquake recurrence.

The COV of earthquake recurrence has been widely used in paleoseismology studies, for example, on the Dead Sea Fault (Marco et al., 1996), southern San Andreas Fault (Scharer et al., 2010), and Alpine Fault in New Zealand (Berryman et al., 2012). In the entire PZ1 outcrop (60–14 ka), the  $\text{COV} = 1.2$ , and thus indicates a temporal clustering of strong earthquakes in time. The earthquake clusters during the time periods of  $\sim 54$ – $50$  ka and  $\sim 44$ – $33$  ka, are termed as Cluster a and b, respectively (Figure 9).

In core 5017-1, the two  $^{14}\text{C}$  ages at 139.6 m and 115.4 m constrain the age of disturbed Sequence II (137.5–115.9 m) to between  $43.9 \pm 0.72$  ka and  $30.3 \pm 0.26$  ka. Thus, disturbed Sequence II can be correlated to earthquake Cluster b (Figure 9). The age of disturbed Sequence I (153.9–149.4 m) is bracketed to

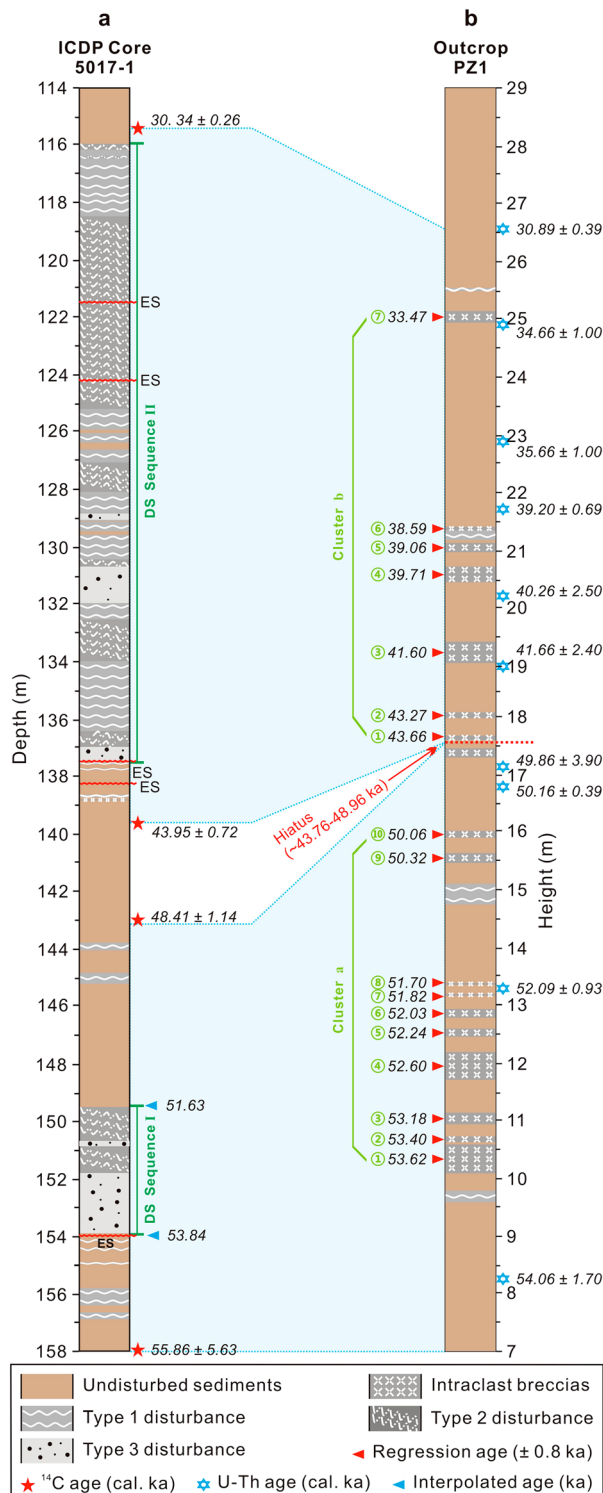


**Figure 9.** Temporal correlation of large-scale disturbances in the Dead Sea depocenter to large earthquake clusters recorded in the Dead Sea margin. (a) Two sequences of large-scale disturbance in the Dead Sea depocenter. (b) Large earthquakes recorded in the Dead Sea margin measured as height (m) above the base of the PZ1 section (Marco et al., 1996). The green numbers mark the large earthquakes that are temporally correlated to the large-scale disturbances in the Dead Sea depocenter. Note the vertical scale in Figure 9b is doubled in comparison to the vertical scale in Figure 9a.

between  $\sim 55.9 \pm 5.6$  ka (157.9 m) and  $49.0 \pm 2.1$  ka (143.0 m) and therefore can be correlated with the earthquake cluster during the  $\sim 59.4$ – $49.2$  ka period in the PZ1 outcrop (Figure 9).

The age of disturbed Sequence I was estimated in detail by linear interpolation, since both the top (149.4 m) and bottom (153.9 m) of the sequence are far ( $>4$  m) from the  $^{14}\text{C}$  ages at 143.0 m and 157.9 m (Figure 9a). The interpolated age spans from  $\sim 54.0$  to  $52.0$  ka, corresponding to the earthquake Cluster a (Figure 9). This age calculation assumes a constant sedimentation rate between the two  $^{14}\text{C}$  age points.

However, the sedimentation rate cannot be constant between 143.0 m and 157.9 m, as the  $\sim 4.5$  m of Type 2 and Type 3 disturbance is part of this core interval. If we assume that Sequence I is one instantaneous event, then the age of the top and bottom of the disturbed Sequence I will be the same, at  $\sim 52.6 \pm 3.9$  ka. Therefore, the most likely real age of disturbed Sequence I is estimated close to  $\sim 52.6$  ka, in line with the linear interpolated age of  $\sim 54.0$ – $52.0$  ka and can still be correlated to earthquake Cluster a (Figure 9). Moreover, due to the uncertainty of the linear interpolated age, the temporal correlation between the depocenter disturbances and onshore large earthquake records is conducted as a package rather than individual events.

## 5. Discussion

### 5.1. Implications of Sedimentary Structures in Three Basic Types of Disturbance

1. Type 1: in situ deformation. The excellent preservation of aragonite laminae in folds (Figure 5) indicates that the units are deformed in situ and have not undergone any significant transportation. More significant movement would disaggregate and destroy the delicate aragonite laminae.
2. Type 2: slump. The poor preservation and fragmentation of aragonite laminae within these sediments (Figure 6) implies that the deformed units are slumped and have undergone significant transportation distances. The features of plastic flow (Figure 6) in these units also support this inference. The lack of coarse sand or gravel in these sediments suggests that these units most probably were sourced from the lake slope area (between the lakeshore and lake center) and underwent a much shorter transportation distance than the Type 3 sediments (discussed below).
3. Type 3: chaotic deposits. The chaotic structure in these sediments (Figure 7) indicates that these units may have undergone a longer transportation distance than other types. Furthermore, the abundant coarse sands and gravels reveals that these chaotic deposits were sourced from the lakeshore areas, where sands and gravels are more commonly deposited.

### 5.2. Determining the Trigger of Large-Scale Disturbances in the Lake Depocenter

The location of the Dead Sea in the central part of the Dead Sea Transform, a seismically active zone, makes a seismic triggering of the meter-scale late Pleistocene disturbances very probable. Moreover, seismic triggered disturbance (e.g., slumps and folds) in different scales are widely observed on both the eastern (El-Isa & Mustafa, 1986; Seilacher, 1984) and western

margin (Alsop & Marco, 2011; Enzel et al., 2000; Kagan et al., 2011; Ken-Tor et al., 2001; Marco & Agnon, 1995; Marco et al., 1996; Migowski et al., 2004) of the Dead Sea.

However, for this case study from the Dead Sea depocenter, nonseismic triggers such as tides (Greb & Archer, 2007), storm waves (Molina et al., 1998), overloading of slope sediments (Moretti et al., 2001; Moretti & Sabato, 2007), and fluvial floods (Li et al., 1996) can be excluded for the following reasons.

#### 5.2.1. Storm Waves and Lake Level Fluctuations

Observations in the Dead Sea reveal that typical amplitudes of winter storm waves are less than 2 m (Nehorai et al., 2013; Sirkes et al., 1997). Lake Lisan's lowest water level is much higher than the present Dead Sea (Torfstein et al., 2013). Water depth at the center of Lake Lisan was at least ~200 m (Begin et al., 1974) and possibly reached up to ~600 m (Katz et al., 1977). Such deep water in the central lake area means that sediments in the depocenter will remain unaffected by storm waves or lake level fluctuations directly.

#### 5.2.2. Flash Flood and Turbidity Current

Modern offshore sedimentation monitoring in the Dead Sea by satellite observations (Nehorai et al., 2013) reveals that flash floods play a key role in supplying suspension particles to the deepwater environment. Closer to the shore, the plume generated by the flood floats above the underlying denser brine (density:  $1.24 \text{ g/cm}^3$ ) forming a hypopycnal flow. With time, the plume dissipates and sinks, unloading fine particles toward the deeper lake environment. During 24 May 1981 to 23 May 1982, sediment traps were deployed in the Dead Sea center at water depths of 70, 120, 170, 220, and 270 m, which captured annual sediment accumulation rates of 24.1, 26.9, 30.1, 33.6, and  $31.7 \text{ mg/cm}^3/\text{yr}$ , respectively (Stiller et al., 1997). Similarity in the sediment accumulation rates measured at different water depths indicates that hypopycnal flows might have been an important process in charge of supplying sediments to the lake depocenter. These suspension particles are eventually deposited to create the millimeter-scale detritus laminae and homogeneous mud in the lake center.

The 2 m thick homogenous units that overlay the two disturbed sequences may be linked to seismic activity, as homogenites have typically been described in association with earthquake-triggered resuspended sediment (McHugh et al., 2011, 2006; Polonia et al., 2016). However, neither the sedimentary structure nor the  $\mu\text{XRF}$  data (Figures 4a and 4b) indicate that the homogenites are disturbed units. More detailed discussion on the homogenites is outside the scope of the present study.

Under some exceptional circumstances, extreme floods with high energy may carry large amounts of coarse particles into the lake and form dense hyperpycnal flows, which can trigger turbidity currents near the lake floor and thereby induce disturbances (Baas et al., 2014; Hsü, 1989). Nevertheless, in our studied core record, the turbidite layers do not show evidence of erosion at their base. Alternating aragonite-detritus laminae that are preserved below these turbidites are not disturbed (Figures 5f–5h). Thus, the thick disturbed Sequences I and II are unlikely to be induced by flash flood-turbidity currents.

#### 5.2.3. Sediment Overloading

This process has been shown to induce instability and disruption of underlying sediments (Moretti et al., 2001; Moretti & Sabato, 2007). The Dead Sea marginal area has much lower sediment accumulation rates than the depocenter. For example, during the last glacial period, the mean sediment accumulation rate in the PZ1 outcrop (Figure 1b) was  $\sim 0.7 \text{ mm yr}^{-1}$ , which is about half of the rate preserved in core 5017-1 ( $\sim 1.4 \text{ mm yr}^{-1}$ ) (Lu et al., 2017). During the Holocene, the mean sediment accumulation rate in the Ein Gedi core (Figure 1d;  $\sim 10\text{--}0 \text{ ka}$ ) was  $\sim 2.1 \text{ mm yr}^{-1}$  (Migowski et al., 2004), which is 3 times lower than in core 5017-1 ( $\sim 7.8 \text{ mm yr}^{-1}$ ) for the same time period.

Furthermore, the Dead Sea marginal area has a much higher sediment accumulation rate during the Holocene interval ( $\sim 2.1 \text{ mm yr}^{-1}$  in the Ein Gedi core) than during the last glacial period ( $\sim 0.7 \text{ mm yr}^{-1}$  in the PZ1 outcrop). However, during the Holocene, no thick ( $>1 \text{ m}$ ) disturbances are identified in core 5017-1. Therefore, the thick disturbed Sequences I and II are unlikely to be produced by sediment overloading, as relatively low sedimentation rates prevailed in the Dead Sea margin area during the last glacial period.

#### 5.2.4. Drilling Deformation

It is reasonable to develop angular discordances across artificial breaks in the studied core interval, since the section was drilled with rotary tools (Stein et al., 2011). However, the thick disturbed Sequences I and II are unlikely to be formed by this artificial drilling-related deformation. This is because (i) the artificial deformation just acted as a secondary localized agent on the original deformation and (ii) the intervals of angular



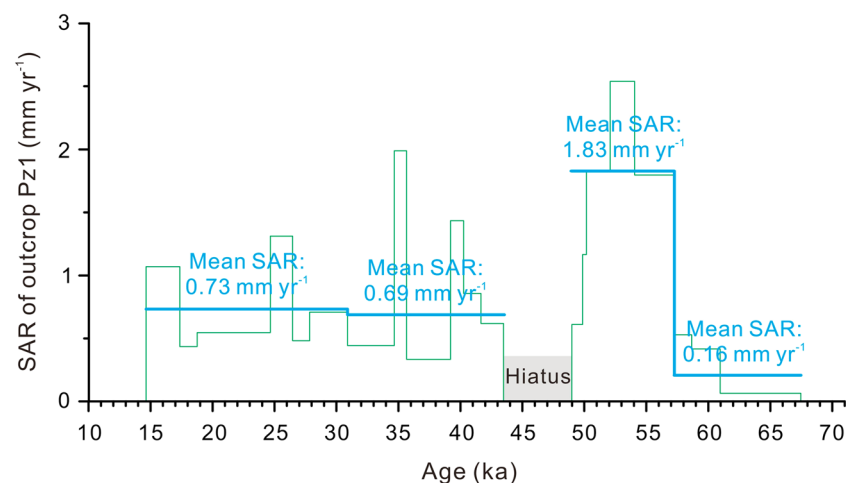


**Figure 10.** Sediment accumulation rate (SAR) in the PZ1 outcrop during ~70–14 ka. The histograms (green line) represent SAR based on age anchors that are used for age models (Haase-Schramm et al., 2004). The bold light blue lines represent mean SAR during several longer time periods. The hiatus is marked by a gray box.

discordance (~5–10 cm spacing) are much thinner and only a small part of each thicker (tens of centimeters to meters thick) deformed unit within the two disturbed sequences.

#### 5.2.5. Seismicity as a Potential Trigger

Extensive exposures of folded layers, slumps (El-Isa & Mustafa, 1986; Seilacher, 1984; Wetzler, Marco, & Heifetz, 2010), and intraclast breccia layers (Alsop & Marco, 2012a, 2012b; Marco & Agnon, 1995, 2005; Marco et al., 1996) were formed in the Lisan Fm at the Dead Sea margins and have been interpreted as seismites in relation to the seismic activity of the Dead Sea Fault. The two disturbed sequences in core 5017-1 are temporally correlated with two earthquake clusters recorded in the Dead Sea marginal area (PZ1 outcrop), supporting strongly an earthquake triggering mechanism for the disturbances.

It should be noted that only part of paleoearthquakes are recorded by intraclast breccia layers in the PZ1 outcrop. During the ~53.6–50.0 ka interval, 10 intraclast breccia layers are observed, yielding a mean recurrence interval of ~360 years. While only seven intraclast breccia layers are observed during the ~43.7–33.5 ka period, hence yielding a recurrence interval of ~1460 years. These mean intervals are both longer than the earthquake mean recurrence interval of ~100 years for the last 4 kyr as calculated from the Ein Gedi Core (Figure 1d) (Migowski et al., 2004). However, the studies of the Dead Sea Transform reveal that the relative slip rate during the late Quaternary converges at around 4–5 mm yr<sup>-1</sup> (Marco & Klinger, 2014). This indicates that the intraclast breccia layers in the PZ1 outcrop only recorded the strongest earthquakes.

Agnon et al. (2006) proposed that the resolution of earthquakes in a lacustrine record can be limited by the detection limit of individual breccia layers. In the PZ1 outcrop, the thinnest breccia layer is ~2 cm, which is observed by the naked eye (Agnon et al., 2006; Marco et al., 1996). However, in the Ein Gedi Core, the thinnest breccia layer is ~2 mm (Migowski et al., 2004), which is observed by microscope. Thus, the earthquake records in the PZ1 outcrop, especially during the period of ~43.8–30.9 ka (Cluster b in Figure 9b), is perhaps incomplete as observations are made by naked eye in the field rather than by detailed microscope analyses.

Another important factor to consider is sediment accumulation rate at the study site (Agnon et al., 2006). Previous studies in the Western Alps suggest that lakes with high sedimentation rates may be much more sensitive to earthquake shaking than those with low sedimentation rates (Wilhelm et al., 2016). The mean sediment accumulation rate in the PZ1 outcrop during the period of ~43.8–30.9 ka was ~0.7 mm yr<sup>-1</sup>, while it reached ~1.8 mm yr<sup>-1</sup> during the period of ~57.3–49.0 ka (Figure 10). We suggest that the extremely low sediment accumulation rate occurring between ~43.8 and 30.9 ka may have reduced the sensitivity of the sediments to earthquake shaking. Hence, some earthquakes may not be recorded during the period ~43.8–30.9 ka (Cluster b in Figure 9b) in the PZ1 outcrop.

Centimeter-scale microfaults have been correlated to historical earthquakes in the Dead Sea (Kagan et al., 2011) and other lake settings (Avşar et al., 2016). Microfaults in the Type 1 disturbance in Sequence II of

core 5017-1 may also suggest some medium to small earthquakes that were not observed from the PZ1 outcrop.

### 5.2.6. Seismic Intensity and Magnitude That May Create Such Disturbances

Previous studies in the PZ1 and Ze'elim outcrop (Figure 1d; late Holocene) suggest that the intraclast breccias are induced by earthquakes with  $M_w > 5.5$  (Ken-Tor et al., 2001; Marco et al., 1996). One folded layer (in situ deformation, 0–0.35 m thick) in the western margin of the Dead Sea (Nahal Darga, Figure 1d) was identified as a result of the Jericho earthquake shaking on 11 July 1927 (Figure 1c) (Enzel et al., 2000). The earthquake had a magnitude of  $M_w$  6.3 and local seismic intensity (MM) between VII and IX. Besides, numerical simulations of in situ deformed layers (0–0.5 m thick) in the Lisan Fm suggest that the local seismic intensity (MM) of VI to IX is needed (Wetzler et al., 2010).

Investigations into the seismic effects of an historical earthquake (year 1601,  $M_w$  6.2) in the Alps of Switzerland suggest that the ~0.4–1.2 m thick slumped layer was induced by local seismic intensity (MM) of VI to VII (Becker et al., 2005; Schnellmann et al., 2002; Schnellmann et al., 2007). Moreover, investigations in instrumental earthquake effects in Comox Lake (British Columbia, Canada) reveal a single ~1 m thick slump layer that was induced by local seismic intensity (MM) of VII to VIII in 1946, with a magnitude of  $M_w$  7.5 (Shilts & Clague, 1992).

In the Nankai Trough, southwest Japan, a chaotic layer was induced by an earthquake with local seismic intensity (MM) of VI–VIII that occurred in 1944 (Sakaguchi et al., 2011). In the Swiss Alps, a ~0.5 m thick chaotic layer was induced by local seismic intensity (MM) of VI–VII (Monecke et al., 2004). Based on these previous worldwide investigations in seismic effects of instrumental, historical, and paleoearthquakes, together with the numerical simulations in the Dead Sea, we suggest that local seismic intensity (MM) of VI is the lower boundary for the creation of in situ deformation, slump, and chaotic deposits under a subaqueous environment.

### 5.3. Seismic Triggering Mechanisms of Large-Scale Disturbances in the Lake Depocenter

Lateral tracing of the in situ deformations (Type 1 disturbance) is limited by the diameter (~6 cm) of the drill core. The complete fold geometry as observed in outcrops in the Dead Sea margin can therefore not be discerned (Figure 5b; supporting information slides). The in situ deformation consists of stratified water-saturated mud and inhibits gravitational Rayleigh–Taylor instabilities that require inverse densities. Heifetz et al. (2005) proposed that earthquake-triggered shear known as the Kelvin–Helmholtz Instability is a plausible mechanism for the soft-sediment deformations in the Lisan Fm, along the western margin of the Dead Sea.

The strong earthquakes may provide shear kinetic energy that exceeds the gravitational potential energy, thereby allowing stratified layers to move horizontally in the same direction but with different velocities thus creating shear in the layers' interface (Heifetz et al., 2005; Wetzler et al., 2010). Power spectral analysis conducted by Wetzler et al. (2010) reveals that the geometry of Lisan folds in the western margin of the Dead Sea, obeys a power law similar to Kelvin–Helmholtz turbulence in other environments. The in situ deformations in the Dead Sea center can be explained by the same mechanism of earthquake-triggered Kelvin–Helmholtz Instability (Figure 11).

Earthquake-triggered subaqueous sediment failure and mass transport from the slope area are widely documented (McHugh et al., 2016, 2011; Papatheodorou & Ferentinos, 1997; Piper et al., 1999; Praet et al., 2017; Van Daele et al., 2015). Sediment failure and mass flows are commonly observed in slopes areas with slope gradient  $< 15^\circ$ , for example, Lake Puyehue in South Central Chile (Moernaut et al., 2007), Lake Lucerne in central Switzerland (Strasser et al., 2010) and Skilak Lake in south central Alaska (Praet et al., 2017). Moreover, seismogenic sediment failures are observed as well in areas characterized by gentle slopes ( $< 1^\circ$ ), such as the Klamath River delta in California (Field et al., 1982) and the western margin of the Dead Sea (Lake Lisan) (Alsop & Marco, 2013).

The slumps and chaotic deposits in the Dead Sea depocenter (Type 2 and Type 3 disturbances, respectively) can be explained by a similar mechanism of earthquake-triggered slope instability. In the present Dead Sea, alluvial fans are developed in the western margin and can supply coarse materials (e.g., gravel) to the depocenter (Figure 11). Slope angles in the lateral margins of the basin are in the range of ~5–20°, which

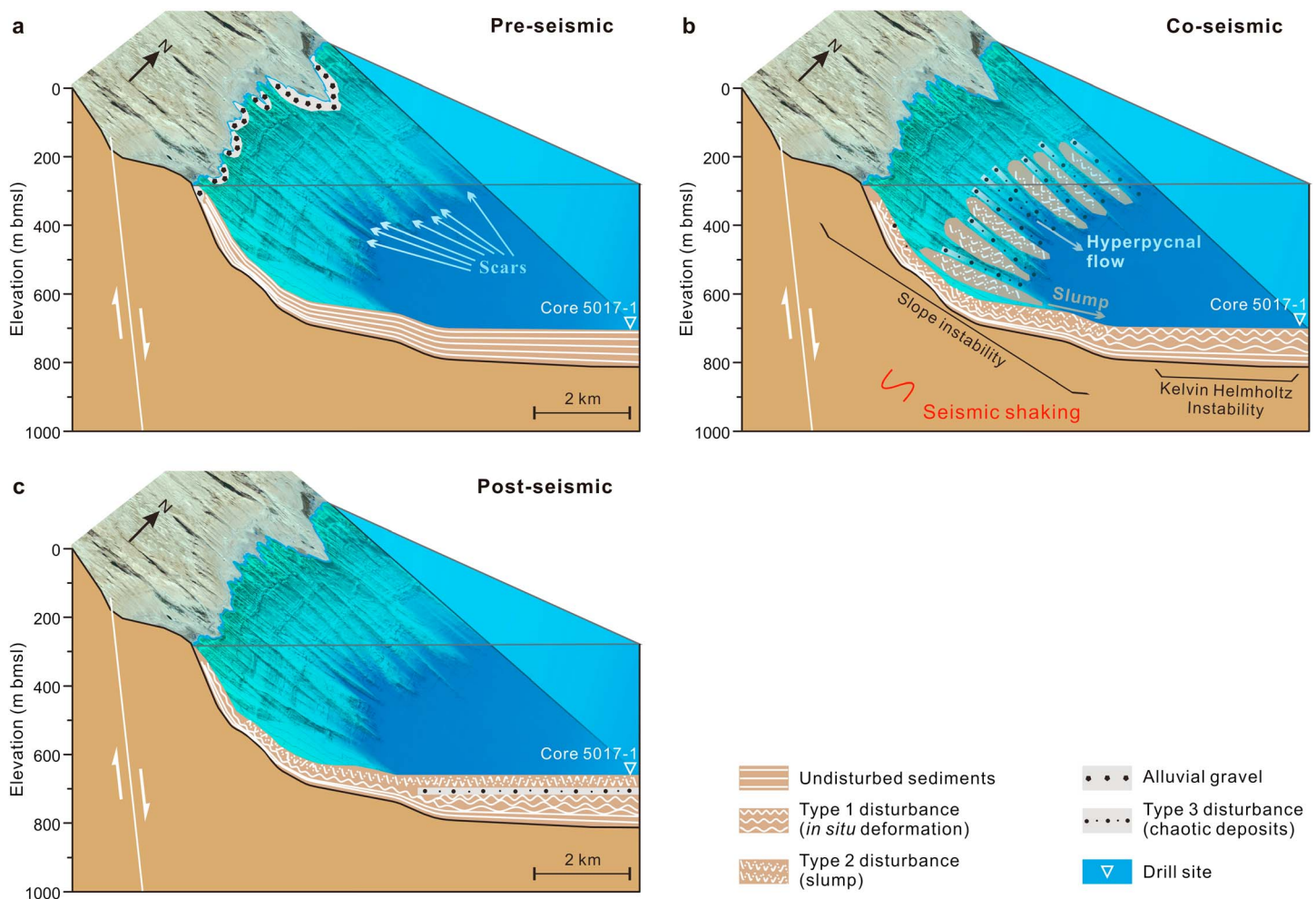


**Figure 11.** Schematic model showing the response of sedimentary processes in a lake depocenter to seismic shaking in a tectonically active region such as the Dead Sea. (a) Preseismic shaking. (b) Coseismic shaking; slope instability and Kelvin-Helmholtz instability are initiated during the shaking. (c) Postseismic shaking. See the text for a detailed interpretation.

are very conducive to developing subaqueous sediment failure and energetic hyperpycnal flows during earthquake shaking. This present Dead Sea morphological setting (Figure 11) can serve as a reasonable analogue for the configuration of the late Pleistocene Lake Lisan.

Moreover, another significant geomorphic feature is the scars that are widely distributed on the slope along the western margin of the lake (Figures 1d and 11). These previously developed scars can serve as natural conveying paths for the energetic downslope transport of nearshore alluvial sediments resulting in the chaotic deposits (McHugh et al., 2002). The pristine lower slope areas (in between the scars) may serve as source areas and transport paths of the slumps.

An ideal succession of in situ deformation (Type 1, at the bottom), chaotic deposits (Type 3, in the middle), and slump (Type 2 on the top) are shown in the model (Figure 11c) of seismic shaking. In situ deformation is commonly missing from the succession because it may be eroded by the energetic transportation of chaotic deposits. This is supported by the observation that intraclasts of deformed laminae are incorporated into the chaotic deposits (Figures 7a–7d).

However, it should be noted that the ideal succession comprising three types of disturbance (i.e., three different disturbed units) does not always represent a single earthquake event. This is because in some cases, a single disturbed unit, for example, the thick in situ deformation, contains evidence of multiple earthquake events. This is an important reason for conducting a correlation of event packages rather than individual events between the depocenter disturbances (in core 5017-1) and the onshore large earthquake records



(in the PZ1 outcrop). Moreover, some erosion surfaces are developed within a thick slumped unit (e.g., the unit between ~125.2 and 118.5 m; Figure 9). Such amalgamation of slumps may indicate a succession of multiple earthquakes, or alternatively multiple synchronous failures along the basin periphery triggered by a single earthquake (Van Daele et al., 2017). However, here the latter can be excluded as only the western slopes seem to be potential sources for these slumps.

The factor of rapid lake level fluctuation should also be considered. Lake level changes will affect the water depth in the slope areas and thus change the hydrostatic pressure applied on the sediments (Moernaut et al., 2010). The lake level fluctuation is the primary factor to increase slope instability in the Dead Sea slope areas. During the studied time period of ~56–30 ka, the lake level fluctuated between –330 and –180 m, in contrast to fluctuation between –440 and –370 m of the Holocene lake level (Bartov et al., 2002; Torfstein et al., 2013). The relatively high-amplitude lake level fluctuation during the studied time period will cause high-amplitude pressure variation in the slope areas that may reduce slope stability (Smith et al., 2013). Thus, we predict that earthquakes with  $M_w > 5.5$  or local seismic intensity (MM)  $> VI$  (section 5.2) recorded in the depocenter core initiated the meter thick slumps and chaotic deposits. This interpretation is in line with our observation that no thick ( $>1$  m) slumps and chaotic deposits are developed in the depocenter core during the Holocene, though earthquakes occurred in this interval (Begin et al., 2005; Migowski et al., 2004).

In the case study, the drilling-related angular discordances across artificial breaks do not affect the model and interpretations described above, since (i) artificial breaks are secondary features superimposed on the original seismic deformation, (ii) they affect relatively small parts (~5–10 cm intervals) of one thick (tens of centimeters to meter thick) seismically deformed unit (in situ deformation or slump).

Limitations of linking a single onshore outcrop (PZ1) with one depocenter drill core through late Pleistocene sediments is apparent. First, the resolution ( $\sim \pm 0.5$ –5 kyr) of dating methods ( $^{14}\text{C}$  and U-Th) are themselves not precise enough to link individual events between the two sites. Second, the central location of the depocenter core may record movement of many faults that surround the Dead Sea Basin, rather than the PZ1 outcrop positioned adjacent to faults on the western margin. Therefore, it may be that only large earthquakes can be correlated between the two sites. Third, we should not expect each slumped layer in the depocenter core to be traced to the PZ1 outcrop, because the depocenter core is located in the northern sub-basin, while the PZ1 outcrop is positioned in the southern subbasin (Figure 1b). Also, it should be noted that depocenters might migrate through time, as described, for example, by Carton et al. (2007) for the Cinarcik Basin, Marmara Sea. Finally, the resolution of present reflection seismic data across the drill core is not good enough to trace each slumped horizon or other disturbance.

Our study case has wide implications for understanding the disturbances and related paleoseismology in seismically active lake depocenters. Being the ultimate repository for mass-transport deposits, depocenters contain the most complete record of earthquakes. This is different to a slope or shelf environment where parts of the record might be eroded.

Slumps and folds were previously observed in sediments from the center of lakes in the Alps (Monecke et al., 2004; Strasser, Monecke, et al., 2013), eastern Turkey (Cukur et al., 2014), South Central Chile (Van Daele et al., 2015), and Patagonia (Waldmann et al., 2011). However, earthquake-triggered large-scale (several meters thick) disturbances as observed in the Dead Sea case study are rarely reported in other areas of the Earth. Under tectonically active conditions, large scale mass-transport disturbances, which are deposited and preserved in the lake's depocenter interfere with obtaining credible ages from the disturbed sediments. Under such conditions, our case study suggests that the long sequence of disturbances can be used to infer earthquake clusters.

## 6. Conclusions

Disruption of unlithified sediments in the Dead Sea margin provides a valuable archive of earthquakes during the past ~70 kyr. However, to date, we know little about disturbances in the basin depocenter, where the water depth is hundreds of meters. The comparison between exposed shallower lake sediments and depocenter drill core is based on temporal correlation. Two sequences of seismically triggered large-scale disturbance in the Dead Sea depocenter are identified. The sequences are composed of three basic types of disturbance: in situ deformation, slump, and chaotic deposits.

The comparison allows us to discern the characteristics of disturbance in the different subaqueous environments and identify the source and sedimentary process of mass transport deposits. Our observations and interpretations indicate that (i) earthquake-triggered Kelvin-Helmholtz Instability is a plausible mechanism for the in situ deformation in the Dead Sea depocenter, (ii) the slumps are slope area sourced, (iii) chaotic deposits are lakeshore sourced, and (iv) earthquake-triggered slope instability is the mechanism that creates slump and chaotic deposits. We further suggest that long disturbance sequences in a seismically active lake depocenter can be used to infer earthquake clustering, since the two disturbance sequences in the depocenter core are temporally correlated to two earthquake clusters in the outcrop.

## Acknowledgments

We thank the funding agencies for this project: the International Continental Scientific Drilling Program (ICDP) and the Israel Science Foundation (ISF; Center of Excellence grant 1436/14 to S. M.). Y. L. is grateful to the Faculty of Exact Sciences in Tel Aviv University for the Postdoctorate Fellowship. We thank Or M. Bialik for help with using the Corelyzer software and Nimer Taha for help with lab work. We thank Cecilia McHugh, Maarten Van Daele, and Associate Editor Brandon Dugan for their constructive comments, which improved the quality of the manuscript substantially. We thank Editor Uri ten Brink for handling this manuscript. Special thanks to Maarten Van Daele for help with identification the artificial deformation structures (the contribution is shown as supporting information, Slide S1). Supporting information in the form of figures and Powerpoint is provided in the electronic supplement. All of the numerical information is provided in the figures in the paper.

## References

- Agnon, A., Migowski, C., & Marco, S. (2006). Intracast breccias in laminated sequences reviewed: Recorders of paleo-earthquakes. *Geological Society of America Special Papers*, 401, 195–214. [https://doi.org/10.1130/2006.2401\(13\)](https://doi.org/10.1130/2006.2401(13))
- Alsop, G. I., & Marco, S. (2011). Soft-sediment deformation within seismogenic slumps of the Dead Sea basin. *Journal of Structural Geology*, 33(4), 433–457. <https://doi.org/10.1016/j.jsg.2011.02.003>
- Alsop, G. I., & Marco, S. (2012a). A large-scale radial pattern of seismogenic slumping towards the Dead Sea Basin. *Journal of the Geological Society*, 169(1), 99–110. <https://doi.org/10.1144/0016-76492011-032>
- Alsop, G. I., & Marco, S. (2012b). Tsunami and seiche-triggered deformation within offshore sediments. *Sedimentary Geology*, 261–262, 90–107. <https://doi.org/10.1016/j.sedgeo.2012.03.013>
- Alsop, G. I., & Marco, S. (2013). Seismogenic slump folds formed by gravity-driven tectonics down a negligible subaqueous slope. *Tectonophysics*, 605, 48–69. <https://doi.org/10.1016/j.tecto.2013.04.004>
- Alsop, G. I., Marco, S., Levi, T., & Weinberger, R. (2017). Fold and thrust systems in Mass Transport Deposits. *Journal of Structural Geology*, 94, 98–115. <https://doi.org/10.1016/j.jsg.2016.11.008>
- Alsop, G. I., Weinberger, R., Marco, S., & Levi, T. (2017). Identifying soft-sediment deformation in rocks. *Journal of Structural Geology*. <https://doi.org/10.1016/j.jsg.2017.09.001>
- Al-Zoubi, A., & ten Brink, U. (2002). Lower crustal flow and the role of shear in basin subsidence: An example from the Dead Sea basin. *Earth and Planetary Science Letters*, 199(1–2), 67–79. [https://doi.org/10.1016/S0012-821X\(02\)00540-X](https://doi.org/10.1016/S0012-821X(02)00540-X)
- Ambraseys, N. (2009). *Earthquakes in the Mediterranean and Middle East: A multidisciplinary study of seismicity up to 1900*. Cambridge: Cambridge University Press. <https://doi.org/10.1017/CBO9781139195430>
- Amiran, D. H., Arieh, E., & Turcotte, T. (1994). Earthquakes in Israel and adjacent areas: Macroseismic observations since 100 BCE. *Israel Exploration Journal*, 260–305.
- Avşar, U., Jónsson, S., Avşar, Ö., & Schmidt, S. (2016). Earthquake-induced soft-sediment deformations and seismically amplified erosion rates recorded in varved sediments of Köyceğiz Lake (SW Turkey). *Journal of Geophysical Research: Solid Earth*, 121, 4767–4779. <https://doi.org/10.1002/2016JB012820>
- Baas, J. H., Manica, R., Puhl, E., Verhagen, I., & de O Borges, A. L. (2014). Processes and products of turbidity currents entering soft muddy substrates. *Geology*, 42(5), 371–374. <https://doi.org/10.1130/g35296.1>
- Babonneau, N., Cattaneo, A., Ratzov, G., Déverchère, J., Yelles-Chauouche, A., Lateb, T., & Bachir, R. S. (2017). Turbidite chronostratigraphy off Algiers, central Algerian margin: A key for reconstructing Holocene paleo-earthquake cycles. *Marine Geology*, 384, 63–80. <https://doi.org/10.1016/j.margeo.2016.10.017>
- Bartov, Y., Stein, M., Enzel, Y., Agnon, A., & Reches, Z. (2002). Lake levels and sequence stratigraphy of Lake Lisan, the late Pleistocene precursor of the Dead Sea. *Quaternary Research*, 57(01), 9–21. <https://doi.org/10.1006/qres.2001.2284>
- Bartov, Y., Steinitz, G., Eyal, M., & Eyal, Y. (1980). Sinistral movement along the Gulf of Aqaba—Its age and relation to the opening of the Red Sea. *Nature*, 285(5762), 220–222. <https://doi.org/10.1038/285220a0>
- Becker, A., Ferry, M., Monecke, K., Schnellmann, M., & Giardini, D. (2005). Multiarchive paleoseismic record of late Pleistocene and Holocene strong earthquakes in Switzerland. *Tectonophysics*, 400(1–4), 153–177. <https://doi.org/10.1016/j.tecto.2005.03.001>
- Begin, Z. B., Ehrlich, A., & Nathan, Y. (1974). Lake Lisan the Pleistocene precursor of the Dead Sea. *Geological Survey of Israel, Bulletin*, 63, 1–30.
- Begin, Z. B., Steinberg, D. M., Ichinose, G. A., & Marco, S. (2005). A 40,000 year unchanging seismic regime in the Dead Sea rift. *Geology*, 33(4), 257–260. <https://doi.org/10.1130/G21115.1>
- Ben-Menahem, A. (1991). Four thousand years of seismicity along the Dead Sea Rift. *Journal of Geophysical Research*, 96(B12), 20,195–20,216. <https://doi.org/10.1029/91JB01936>
- Berryman, K. R., Cochran, U. A., Clark, K. J., Biasi, G. P., Langridge, R. M., & Villamor, P. (2012). Major earthquakes occur regularly on an isolated plate boundary fault. *Science*, 336(6089), 1690–1693. <https://doi.org/10.1126/science.1218959>
- Calvo, R., & Bartov, Y. (2001). Hazeva Group, southern Israel: New observations, and their implications for its stratigraphy, paleogeography, and tectono-sedimentary regime. *Israel Journal of Earth Sciences*, 50(2–4), 71–100. <https://doi.org/10.1560/B02L-6K04-UFQL-KUE3>
- Carton, H., Singh, S., Hirn, A., Bazin, S., De Voogd, B., Vigner, A., ... Karakoc, F. (2007). Seismic imaging of the three-dimensional architecture of the Çınarcık basin along the North Anatolian fault. *Journal of Geophysical Research*, 112, B06101. <https://doi.org/10.1029/2006JB004548>
- Cukur, D., Krastel, S., Schmincke, H.-U., Sumita, M., Çağatay, M. N., Meydan, A. F., ... Stockhecke, M. (2014). Seismic stratigraphy of Lake Van, eastern Turkey. *Quaternary Science Reviews*, 104, 63–84. <https://doi.org/10.1016/j.quascirev.2014.07.016>
- El-Isa, Z., & Mustafa, H. (1986). Earthquake deformations in the Lisan deposits and seismotectonic implications. *Geophysical Journal International*, 86(2), 413–424. <https://doi.org/10.1111/j.1365-246X.1986.tb03835.x>
- Enzel, Y., Kadan, G., & Eyal, Y. (2000). Holocene earthquakes inferred from a fan-delta sequence in the Dead Sea graben. *Quaternary Research*, 53(01), 34–48. <https://doi.org/10.1006/qres.1999.2096>
- Field, M. E., Gardner, J. V., Jennings, A. E., & Edwards, B. D. (1982). Earthquake-induced sediment failures on a 0.25° slope, Klamath River delta, California. *Geology*, 10(10), 542–546. [https://doi.org/10.1130/0091-7613\(1982\)10%3C542:EFOAS%3E2.0.CO;2](https://doi.org/10.1130/0091-7613(1982)10%3C542:EFOAS%3E2.0.CO;2)
- Freund, R., Zak, I., & Garfunkel, Z. (1968). Age and rate of the sinistral movement along the Dead Sea Rift. *Nature*, 220(5164), 253–255. <https://doi.org/10.1038/220253a0>
- Garfunkel, Z. (1981). Internal structure of the Dead Sea leaky transform (rift) in relation to plate kinematics. *Tectonophysics*, 80(1–4), 81–108. [https://doi.org/10.1016/0040-1951\(81\)90143-8](https://doi.org/10.1016/0040-1951(81)90143-8)

- Garfunkel, Z. (2009). The long-and short-term lateral slip and seismicity along the Dead Sea Transform: An interim evaluation. *Israel Journal of Earth Sciences*, 58(3), 217–235. <https://doi.org/10.1560/IJES.58.3-4.217>
- Garfunkel, Z. (2014). Lateral motion and deformation along the Dead Sea transform. In Z. Garfunkel, Z. Ben-Avraham, & E. Kagan (Eds.), *Dead Sea transform fault system: Reviews* (pp. 109–150). Dordrecht: Springer.
- Garfunkel, Z., & Ben-Avraham, Z. (1996). The structure of the Dead Sea basin. *Tectonophysics*, 266(1–4), 155–176. [https://doi.org/10.1016/S0040-1951\(96\)00188-6](https://doi.org/10.1016/S0040-1951(96)00188-6)
- Gladkov, A. S., Lobova, E. U., Deev, E. V., Korzhnikov, A. M., Mazeika, J. V., Abdieva, S. V., ... Yudakhin, A. S. (2016). Earthquake-induced soft-sediment deformation structures in Late Pleistocene lacustrine deposits of Issyk-Kul lake (Kyrgyzstan). *Sedimentary Geology*, 344, 112–122. <https://doi.org/10.1016/j.sedgeo.2016.06.019>
- Greb, S. F., & Archer, A. W. (2007). Soft-sediment deformation produced by tides in a meizoseismic area, Turnagain Arm, Alaska. *Geology*, 35(5), 435. <https://doi.org/10.1130/g23209a.1>
- Haase-Schramm, A., Goldstein, S. L., & Stein, M. (2004). U-Th dating of Lake Lisan (late Pleistocene dead sea) aragonite and implications for glacial east Mediterranean climate change. *Geochimica et Cosmochimica Acta*, 68(5), 985–1005. <https://doi.org/10.1016/j.gca.2003.07.016>
- Heifetz, E., Agnon, A., & Marco, S. (2005). Soft sediment deformation by Kelvin Helmholtz Instability: A case from Dead Sea earthquakes. *Earth and Planetary Science Letters*, 236(1–2), 497–504. <https://doi.org/10.1016/j.epsl.2005.04.019>
- Hsü, K. J. (1989). *Physical principles of sedimentology: A readable textbook for beginners and experts*. Berlin: Springer. <https://doi.org/10.1007/978-3-662-02584-0>
- Jiang, H., Zhong, N., Li, Y., Xu, H., Yang, H., & Peng, X. (2016). Soft sediment deformation structures in the Lixian lacustrine sediments, eastern Tibetan Plateau and implications for postglacial seismic activity. *Sedimentary Geology*, 344, 123–134. <https://doi.org/10.1016/j.sedgeo.2016.06.011>
- Kagan, E. J., Agnon, A., Bar-Matthews, M., & Ayalon, A. (2005). Dating large infrequent earthquakes by damaged cave deposits. *Geology*, 33(4), 261. <https://doi.org/10.1130/g21193.1>
- Kagan, E. J., Stein, M., Agnon, A., & Neumann, F. (2011). Intrabasin paleoearthquake and quiescence correlation of the late Holocene Dead Sea. *Journal of Geophysical Research*, 116, B04311. <https://doi.org/10.1029/2010JB007452>
- Kagan, Y. Y., & Jackson, D. D. (1991). Long-term earthquake clustering. *Geophysical Journal International*, 104(1), 117–134. <https://doi.org/10.1111/j.1365-246X.1991.tb02498.x>
- Katz, A., Kolodny, Y., & Nissenbaum, A. (1977). The geochemical evolution of the Pleistocene Lake Lisan—Dead Sea system. *Geochimica et Cosmochimica Acta*, 41(11), 1609–1626. [https://doi.org/10.1016/0016-7037\(77\)90172-7](https://doi.org/10.1016/0016-7037(77)90172-7)
- Ken-Tor, R., Agnon, A., Enzel, Y., Stein, M., Marco, S., & Negendank, J. F. W. (2001). High-resolution geological record of historic earthquakes in the Dead Sea basin. *Journal of Geophysical Research*, 106(B2), 2221–2234. <https://doi.org/10.1029/2000JB900313>
- Kitagawa, H., Stein, M., Goldstein, S. L., Nakamura, A., Lazar, B., & Party, D. S. (2017). Radiocarbon chronology of the DSDP core at the deepest floor of the Dead Sea. *Radiocarbon*, 59(02), 383–394. <https://doi.org/10.1017/RDC.2016.120>
- Klinger, Y., Rivera, L., Haessler, H., & Maurin, J.-C. (1999). Active faulting in the Gulf of Aqaba: New knowledge from the  $M_w$  7.3 earthquake of 22 November 1995. *Bulletin of Seismological Society of America*, 89(4), 1025–1036.
- Li, Y., Craven, J., Schweig, E. S., & Obermeier, S. F. (1996). Sand boils induced by the 1993 Mississippi River flood: Could they one day be misinterpreted as earthquake-induced liquefaction? *Geology*, 24(2), 171–174. [https://doi.org/10.1130/0091-7613\(1996\)024%3C0171:SBIBTM%3E2.3.CO;2](https://doi.org/10.1130/0091-7613(1996)024%3C0171:SBIBTM%3E2.3.CO;2)
- Liu-Zeng, J., Shao, Y., Klinger, Y., Xie, K., Yuan, D., & Lei, Z. (2015). Variability in magnitude of paleoearthquakes revealed by trenching and historical records, along the Haiyuan Fault, China. *Journal of Geophysical Research: Solid Earth*, 120, 8304–8333. <https://doi.org/10.1002/2015JB012163>
- Lu, Y., Waldmann, N., Nadel, D., & Marco, S. (2017). Increased sedimentation following the Neolithic Revolution in the Southern Levant. *Global and Planetary Change*, 152, 199–208. <https://doi.org/10.1016/j.gloplacha.2017.04.003>
- Manspeizer, W. (1985). The Dead Sea Rift: Impact of climate and tectonism on Pleistocene and Holocene sedimentation. In K. T. Biddle, & N. Christie-Blick (Eds.), *Strike-slip deformation, basin formation and sedimentation, special publication* (Vol. 37, pp. 143–158). Tulsa, OK: Society for Economic Paleontology and Mineralogy. <https://doi.org/10.2110/pec.85.37.0143>
- Marco, S., & Agnon, A. (1995). Prehistoric earthquake deformations near Masada, Dead Sea graben. *Geology*, 23(8), 695–698. [https://doi.org/10.1130/0091-7613\(1995\)023%3C0695:PEDNMD%3E2.3.CO;2](https://doi.org/10.1130/0091-7613(1995)023%3C0695:PEDNMD%3E2.3.CO;2)
- Marco, S., & Agnon, A. (2005). High-resolution stratigraphy reveals repeated earthquake faulting in the Masada Fault Zone, Dead Sea Transform. *Tectonophysics*, 408(1–4), 101–112. <https://doi.org/10.1016/j.tecto.2005.05.036>
- Marco, S., & Klinger, Y. (2014). Review of on-fault palaeoseismic studies along the Dead Sea Fault. In Z. Garfunkel, Z. Ben-Avraham, & E. Kagan (Eds.), *Dead Sea Transform Fault System: Reviews* (pp. 183–205). Dordrecht: Springer.
- Marco, S., Stein, M., Agnon, A., & Ron, H. (1996). Long-term earthquake clustering: A 50,000 years paleoseismic record in the Dead Sea Graben. *Journal of Geophysical Research*, 101(B3), 6179–6191. <https://doi.org/10.1029/95JB01587>
- McHugh, C. M. G., Braudy, N., Çağatay, M. N., Sorlien, C., Cormier, M.-H., Seeber, L., & Henry, P. (2014). Seafloor fault ruptures along the north Anatolia Fault in the Marmara Sea, Turkey: Link with the adjacent basin turbidite record. *Marine Geology*, 353, 65–83. <https://doi.org/10.1016/j.margeo.2014.03.005>
- McHugh, C. M., Damuth, J. E., & Mountain, G. S. (2002). Cenozoic mass-transport facies and their correlation with relative sea-level change, New Jersey continental margin. *Marine Geology*, 184(3–4), 295–334. [https://doi.org/10.1016/S0025-3227\(01\)00240-7](https://doi.org/10.1016/S0025-3227(01)00240-7)
- McHugh, C. M., Kanamatsu, T., Seeber, L., Bopp, R., Cormier, M.-H., & Usami, K. (2016). Remobilization of surficial slope sediment triggered by the AD 2011  $M_w$  9 Tohoku-Oki earthquake and tsunami along the Japan Trench. *Geology*, 44(5), 391–394. <https://doi.org/10.1130/G37650.1>
- McHugh, C. M., Seeber, L., Braudy, N., Cormier, M.-H., Davis, M. B., Diebold, J. B., ... Templeton, J. (2011). Offshore sedimentary effects of the 12 January 2010 Haiti earthquake. *Geology*, 39(8), 723–726. <https://doi.org/10.1130/g31815.1>
- McHugh, C., Seeber, L., Cormier, M., Dutton, J., Çağatay, N., Polonia, A., ... Gorur, N. (2006). Submarine earthquake geology along the North Anatolia Fault in the Marmara Sea, Turkey: A model for transform basin sedimentation. *Earth and Planetary Science Letters*, 248(3–4), 661–684. <https://doi.org/10.1016/j.epsl.2006.05.038>
- McKEE, E. D., Douglass, J. R., & Rittenhouse, S. (1971). Deformation of lee-side laminae in eolian dunes. *Geological Society of America Bulletin*, 82(2), 359–378. [https://doi.org/10.1130/0016-7606\(1971\)82%5B359:DOLLIE%5D2.0.CO;2](https://doi.org/10.1130/0016-7606(1971)82%5B359:DOLLIE%5D2.0.CO;2)
- Migowski, C., Agnon, A., Bookman, R., Negendank, J. F. W., & Stein, M. (2004). Recurrence pattern of Holocene earthquakes along the Dead Sea transform revealed by varve-counting and radiocarbon dating of lacustrine sediments. *Earth and Planetary Science Letters*, 222(1), 301–314. <https://doi.org/10.1016/j.epsl.2004.02.015>
- Moernaut, J., De Batist, M., Charlet, F., Heirman, K., Chapron, E., Pino, M., ... Urrutia, R. (2007). Giant earthquakes in South-Central Chile revealed by Holocene mass-wasting events in Lake Puyehue. *Sedimentary Geology*, 195(3–4), 239–256. <https://doi.org/10.1016/j.sedgeo.2006.08.005>



- Moernaut, J., Verschuren, D., Charlet, F., Kristen, I., Fagot, M., & De Batist, M. (2010). The seismic-stratigraphic record of lake-level fluctuations in Lake Challa: Hydrological stability and change in equatorial East Africa over the last 140kyr. *Earth and Planetary Science Letters*, 290(1–2), 214–223. <https://doi.org/10.1016/j.epsl.2009.12.023>
- Molina, J., Alfaro, P., Moretti, M., & Soria, J. (1998). Soft-sediment deformation structures induced by cyclic stress of storm waves in tempestites (Miocene, Guadalquivir Basin, Spain). *Terra Nova*, 10(3), 145–150. <https://doi.org/10.1046/j.1365-3121.1998.00183.x>
- Monecke, K., Anselmetti, F. S., Becker, A., Schnellmann, M., Sturm, M., & Giardini, D. (2007). Earthquake-induced deformation structures in lake deposits: A Late Pleistocene to Holocene paleoseismic record for Central Switzerland. *Eclogae Geologicae Helveticae*, 99(3), 343–362. <https://doi.org/10.1007/s00015-006-1193-x>
- Monecke, K., Anselmetti, F. S., Becker, A., Sturm, M., & Giardini, D. (2004). The record of historic earthquakes in lake sediments of Central Switzerland. *Tectonophysics*, 394(1–2), 21–40. <https://doi.org/10.1016/j.tecto.2004.07.053>
- Moretti, M. (2000). Soft-sediment deformation structures interpreted as seismites in middle-late Pleistocene aeolian deposits (Apulian foreland, southern Italy). *Sedimentary Geology*, 135(1–4), 167–179. [https://doi.org/10.1016/S0037-0738\(00\)00070-1](https://doi.org/10.1016/S0037-0738(00)00070-1)
- Moretti, M., & Sabato, L. (2007). Recognition of trigger mechanisms for soft-sediment deformation in the Pleistocene lacustrine deposits of the Sant'Arcangelo Basin (Southern Italy): Seismic shock vs. overloading. *Sedimentary Geology*, 196(1–4), 31–45. <https://doi.org/10.1016/j.sedgeo.2006.05.012>
- Moretti, M., Soria, J. M., Alfaro, P., & Walsh, N. (2001). Asymmetrical soft-sediment deformation structures triggered by rapid sedimentation in turbiditic deposits (Late Miocene, Guadix Basin, southern Spain). *Facies*, 44(1), 283–294. <https://doi.org/10.1007/BF02668179>
- Neev, D., & Emery, K. O. (1967). The Dead Sea, depositional processes and environments of evaporites. *Geological Survey of Israel, Bulletin*, 41, 1–147.
- Nehorai, R., Lensky, I. M., Hochman, L., Gertman, I., Brenner, S., Muskin, A., & Lensky, N. G. (2013). Satellite observations of turbidity in the Dead Sea. *Journal of Geophysical Research: Oceans*, 118, 3146–3160. <https://doi.org/10.1002/jgrc.20204>
- Neugebauer, I., Brauer, A., Schwab, M. J., Waldmann, N. D., Enzel, Y., Kitagawa, H., ... Ariztegui, D. (2014). Lithology of the long sediment record recovered by the ICDP Dead Sea Deep Drilling Project (DSDDP). *Quaternary Science Reviews*, 102, 149–165. <https://doi.org/10.1016/j.quascirev.2014.08.013>
- Owen, G., Moretti, M., & Alfaro, P. (2011). Recognising triggers for soft-sediment deformation: Current understanding and future directions. *Sedimentary Geology*, 235(3–4), 133–140. <https://doi.org/10.1016/j.sedgeo.2010.12.010>
- Papathodorou, G., & Ferentinos, G. (1997). Submarine and coastal sediment failure triggered by the 1995,  $M_s = 6.1$  R Aegion earthquake, Gulf of Corinth, Greece. *Marine Geology*, 137(3–4), 287–304. [https://doi.org/10.1016/S0025-3227\(96\)00089-8](https://doi.org/10.1016/S0025-3227(96)00089-8)
- Pedersen, A., Kocurek, G., Mohrig, D., & Smith, V. (2015). Dune deformation in a multi-directional wind regime: White Sands Dune Field, New Mexico. *Earth Surface Processes and Landforms*, 40(7), 925–941. <https://doi.org/10.1002/esp.3700>
- Piper, D. J., Cochonat, P., & Morrison, M. L. (1999). The sequence of events around the epicentre of the 1929 Grand Banks earthquake: Initiation of debris flows and turbidity current inferred from sidescan sonar. *Sedimentology*, 46(1), 79–97. <https://doi.org/10.1046/j.1365-3091.1999.00204.x>
- Polonia, A., Vaiani, S. C., & de Lange, G. J. (2016). Did the A.D. 365 Crete earthquake/tsunami trigger synchronous giant turbidity currents in the Mediterranean Sea? *Geology*, 44(3), 191–194. <https://doi.org/10.1130/g37486.1>
- Praet, N., Moernaut, J., Van Daele, M., Boes, E., Haeussler, P. J., Strupler, M., ... De Batist, M. (2017). Paleoseismic potential of sublacustrine landslide records in a high-seismicity setting (south-central Alaska). *Marine Geology*, 384, 103–119. <https://doi.org/10.1016/j.margeo.2016.05.004>
- Prasad, S., Vos, H., Negendank, J. F. W., Waldmann, N., Goldstein, S. L., & Stein, M. (2004). Evidence from Lake Lisan of solar influence on decadal- to centennial-scale climate variability during marine oxygen isotope stage 2. *Geology*, 32(7), 581–584. <https://doi.org/10.1130/g20553.1>
- Sade, A., Hall, J., Sade, H., Amit, G., Tibor, G., Schulze, B., ... C. Keller (2014). Multibeam bathymetric map of the Dead Sea, Geological Survey of Israel report GSI/01/2014, Jerusalem, Israel. Retrieved from [http://www.gsi.gov.il/\\_uploads/ftp/Maps/Shaded-batimetry\\_map-Dead-Sea-Poster-Front-300dpi.pdf](http://www.gsi.gov.il/_uploads/ftp/Maps/Shaded-batimetry_map-Dead-Sea-Poster-Front-300dpi.pdf)
- Sakaguchi, A., Kimura, G., Strasser, M., Scream, E. J., Curewitz, D., & Murayama, M. (2011). Episodic seafloor mud brecciation due to great subduction zone earthquakes. *Geology*, 39(10), 919–922. <https://doi.org/10.1130/G32043.1>
- Scharer, K. M., Biasi, G. P., Weldon, R. J., & Fumal, T. E. (2010). Quasi-periodic recurrence of large earthquakes on the southern San Andreas fault. *Geology*, 38(6), 555–558. <https://doi.org/10.1130/g30746.1>
- Schnellmann, M., Anselmetti, F. S., Giardini, D., & McKenzie, J. A. (2007). 15,000 years of mass-movement history in Lake Lucerne: Implications for seismic and tsunami hazards. *Eclogae Geologicae Helveticae*, 99(3), 409–428. <https://doi.org/10.1007/s00015-006-1196-7>
- Schnellmann, M., Anselmetti, F. S., Giardini, D., McKenzie, J. A., & Ward, S. N. (2002). Prehistoric earthquake history revealed by lacustrine slump deposits. *Geology*, 30(12), 1131–1134. [https://doi.org/10.1130/0091-7613\(2002\)030%3C1131:PEHRBL%3E2.0.CO;2](https://doi.org/10.1130/0091-7613(2002)030%3C1131:PEHRBL%3E2.0.CO;2)
- Schramm, A., Stein, M., & Goldstein, S. L. (2000). Calibration of the 14C time scale to > 40 ka by 234U-230Th dating of Lake Lisan sediments (last glacial Dead Sea). *Earth and Planetary Science Letters*, 175(1–2), 27–40. [https://doi.org/10.1016/S0012-821X\(99\)00279-4](https://doi.org/10.1016/S0012-821X(99)00279-4)
- Seilacher, A. (1984). Sedimentary structures tentatively attributed to seismic events. *Marine Geology*, 55(1–2), 1–12. [https://doi.org/10.1016/0025-3227\(84\)90129-4](https://doi.org/10.1016/0025-3227(84)90129-4)
- Shapira, A., Avni, R., & Nur, A. (1993). A new estimate for the epicenter of the Jericho earthquake of 11 July 1927. *Israel Journal of Earth Sciences*, 42(2), 93–96.
- Shilts, W., & Clague, J. J. (1992). Documentation of earthquake-induced disturbance of lake sediments using subbottom acoustic profiling. *Canadian Journal of Earth Sciences*, 29(5), 1018–1042. <https://doi.org/10.1139/e92-084>
- Sims, J. D. (1973). Earthquake-induced structures in sediments of Van Norman Lake, San Fernando, California. *Science*, 182(4108), 161–163. <https://doi.org/10.1126/science.182.4108.161>
- Sims, J. D. (2013). Earthquake-induced load casts, pseudonodules, ball-and-pillow structures, and convolute lamination: Additional deformation structures for paleoseismic studies. *Geological Society of America Special Papers*, 493, 191–201. [https://doi.org/10.1130/2012.2493\(09\)](https://doi.org/10.1130/2012.2493(09))
- Sirkes, Z., Schirmer, F., Essen, H.-H., & Gurgel, K.-W. (1997). Surface currents and seiches in the Dead Sea. In T. M. Niemi, Z. Ben-Avraham, & J. Gat (Eds.), *The Dead Sea: The lake and its setting*, (pp. 104–113). USA: Oxford University Press.
- Smith, D. E., Harrison, S., & Jordan, J. T. (2013). Sea level rise and submarine mass failures on open continental margins. *Quaternary Science Reviews*, 82, 93–103. <https://doi.org/10.1016/j.quascirev.2013.10.012>
- Sneh, A. (1981). The Hazeva formation in the northern Arava, Israel. *Israel Journal of Earth Sciences*, 30(2–3), 81–92.
- Stein, M. (2001). The sedimentary and geochemical record of Neogene-Quaternary water bodies in the Dead Sea Basin-inferences for the regional paleoclimatic history. *Journal of Paleolimnology*, 26(3), 271–282. <https://doi.org/10.1023/A:1017529228186>

- Stein, M., Ben-Avraham, Z., Goldstein, S., Agnon, A., Ariztegui, D., Brauer, A., ... Yasuda, Y. (2011). Deep drilling at the Dead Sea. *Scientific Drilling*, 11, 46–47. <https://doi.org/10.5194/sd-11-46-2011>
- Stein, M., Starinsky, A., Katz, A., Goldstein, S. L., Machlus, M., & Schramm, A. (1997). Strontium isotopic, chemical, and sedimentological evidence for the evolution of Lake Lisan and the Dead Sea. *Geochimica et Cosmochimica Acta*, 61(18), 3975–3992. [https://doi.org/10.1016/S0016-7037\(97\)00191-9](https://doi.org/10.1016/S0016-7037(97)00191-9)
- Stiller, M., Gat, J. R., & Kaushansky, P. (1997). Halite precipitation and sediment deposition as measured in sediment traps deployed in the Dead Sea: 1981–1983. In T. M. Niemi, Z. Ben-Avraham, & J. Gat (Eds.), *The Dead Sea: The lake and its setting* (pp. 171–183). USA: Oxford University Press.
- Strasser, M., Hilbe, M., & Anselmetti, F. S. (2010). Mapping basin-wide subaquatic slope failure susceptibility as a tool to assess regional seismic and tsunami hazards. *Marine Geophysical Research*, 32(1–2), 331–347. <https://doi.org/10.1007/s11001-010-9100-2>
- Strasser, M., Kölling, M., dos Santos Ferreira, C., Fink, H. G., Fujiwara, T., Henkel, S., ... Wefer, G. (2013). A slump in the trench: Tracking the impact of the 2011 Tohoku-Oki earthquake. *Geology*, 41(8), 935–938. <https://doi.org/10.1130/g34477.1>
- Strasser, M., Monecke, K., Schnellmann, M., Anselmetti, F. S., & Weissurt, H. (2013). Lake sediments as natural seismographs: A compiled record of Late Quaternary earthquakes in Central Switzerland and its implication for Alpine deformation. *Sedimentology*, 60(1), 319–341. <https://doi.org/10.1111/sed.12003>
- ten Brink, U. S., & Ben-Avraham, Z. (1989). The anatomy of a pull-apart basin: Seismic reflection observations of the Dead Sea basin. *Tectonics*, 8(2), 333–350. <https://doi.org/10.1029/TC008i002p00333>
- Torfstein, A., Goldstein, S. L., Kushnir, Y., Enzel, Y., Haug, G., & Stein, M. (2015). Dead Sea drawdown and monsoonal impacts in the Levant during the last interglacial. *Earth and Planetary Science Letters*, 412, 235–244. <https://doi.org/10.1016/j.epsl.2014.12.013>
- Torfstein, A., Goldstein, S. L., Stein, M., & Enzel, Y. (2013). Impacts of abrupt climate changes in the Levant from Last Glacial Dead Sea levels. *Quaternary Science Reviews*, 69, 1–7. <https://doi.org/10.1016/j.quascirev.2013.02.015>
- Van Daele, M., Meyer, I., Moernaut, J., De Decker, S., Verschuren, D., & De Batist, M. (2017). A revised classification and terminology for stacked and amalgamated turbidites in environments dominated by (hemi) pelagic sedimentation. *Sedimentary Geology*, 357, 72–82. <https://doi.org/10.1016/j.sedgeo.2017.06.007>
- Van Daele, M., Moernaut, J., Doom, L., Boes, E., Fontijn, K., Heirman, K., ... Trofimovs, J. (2015). A comparison of the sedimentary records of the 1960 and 2010 great Chilean earthquakes in 17 lakes: Implications for quantitative lacustrine palaeoseismology. *Sedimentology*, 62(5), 1466–1496. <https://doi.org/10.1111/sed.12193>
- Van Loon, A. (2009). Soft-sediment deformation structures in siliciclastic sediments: An overview. *Geologos*, 15, 3–55.
- Waldmann, N., Anselmetti, F. S., Ariztegui, D., Austin, J. A. Jr., Pirouz, M., Moy, C. M., & Dunbar, R. (2011). Holocene mass-wasting events in Lago Fagnano, Tierra del Fuego (54°S): Implications for paleoseismicity of the Magallanes-Fagnano transform fault. *Basin Research*, 23(2), 171–190. <https://doi.org/10.1111/j.1365-2117.2010.00489.x>
- Wetzler, N., Marco, S., & Heifetz, E. (2010). Quantitative analysis of seismogenic shear-induced turbulence in lake sediments. *Geology*, 38(4), 303–306. <https://doi.org/10.1130/g30685.1>
- Wilhelm, B., Nomade, J., Crouzet, C., Litty, C., Sabatier, P., Belle, S., ... Anselmetti, F. S. (2016). Quantified sensitivity of small lake sediments to record historic earthquakes: Implications for paleoseismology. *Journal of Geophysical Research: Earth Surface*, 121, 2–16. <https://doi.org/10.1002/2015JF003644>